



## XIX Escola Brasileira de Estrutura Eletrônica

**Excitonic effects using WanTiBEXOS package:  
a MLWF-TB+BSE approach**

**Prof. Dr. Alexandre Cavalheiro Dias (IF-UnB)**

[alexandre.dias@unb.br](mailto:alexandre.dias@unb.br)



<https://wantibexos.readthedocs.io/en/latest/>

<https://github.com/ac-dias/wantibexos>

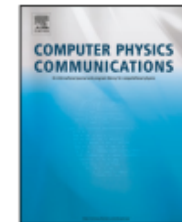
# Actual Publication



Contents lists available at [ScienceDirect](#)

## Computer Physics Communications

journal homepage: [www.elsevier.com/locate/cpc](http://www.elsevier.com/locate/cpc)



# WanTiBEXOS: A Wannier based Tight Binding code for electronic band structure, excitonic and optoelectronic properties of solids



Alexandre C. Dias <sup>a,c,\*</sup>, Julian F.R.V. Silveira <sup>b</sup>, Fanyao Qu <sup>a</sup>

<sup>a</sup> Physical Institute and International Center for Condensed Matter Physics, University of Brasília, Brasília 70919-970, DF, Brazil

<sup>b</sup> Department of Chemical Engineering, Universidade Federal do Rio Grande do Sul, Porto Alegre, Brazil

<sup>c</sup> São Carlos Institute of Chemistry, University of São Paulo, P.O. Box 780, 13560-970, São Carlos, SP, Brazil

### ARTICLE INFO

#### Article history:

Received 8 August 2022

Received in revised form 19 November 2022

Accepted 7 December 2022

Available online 16 December 2022

#### Keywords:

Tight-Binding

Wannier functions

Excitons

Electronic and optical properties

### ABSTRACT

The Bethe-Salpeter equation (BSE) approach becomes a methodology commonly used for simulating excitonic and optical properties in computer materials sciences. However, BSE approach based directly on first principles demands a high computational cost, being prohibitive for larger systems. In order to overcome this challenge, we have developed WanTiBEXOS, a parallel computational FORTRAN code, constituted of a maximally localized Wannier functions based tight-binding (MLWF-TB) model in conjunction with BSE framework. The MLWF-TB Hamiltonian used in WanTiBEXOS package can be obtained via any density functional theory package interfaced with Wannier90 code. It's expected, due MLWF-TB formalism, a computational time reduction around one or more orders of magnitude in comparison with BSE *ab initio* implementations. In order to demonstrate its reliability, flexibility, efficiency and versatility of WanTiBEXOS, we simulate electronic and optical property calculations for the representative materials, including conventional bulk semiconductors, perovskites, nano-monolayer materials and van der Waals heterostructures.

## Developing Team

Main Developer/  
Optical Properties



Prof. Dr. Alexandre  
Cavalheiro Dias  
IF/CIF/UnB

Interfaces with localized  
Basis DFT codes



Dr. Carlos Maciel de  
Oliveira Bastos  
CIF/UnB

Simstack Interface/  
Website



Dr. Celso Ricardo C. Rêgo  
Karlsruhe Institute of  
Technology (Germany)

Debuging and Testing



Prof. Dr. Maurício  
Jeomar Piotrowski  
IFM/GTCMC/  
UFPel



Prof. Dr. Diego  
Guedes-Sobrinho  
IQ/Q<sup>2</sup>M/UFPR

## Developing Team

Thermoelectric  
Properties



Prof. Dr. Elie A.  
Moujaes  
IF/UFBA

Non-linear Optics



Prof. Dr. Teldo Anderson  
da Silva Pereira  
IF/UFMT

GW and Non-linear  
Optics



Msc. Luiz Gustavo  
Tenório  
ITA/ Tohoku University

Extended Huckel  
Tight Binding Interface

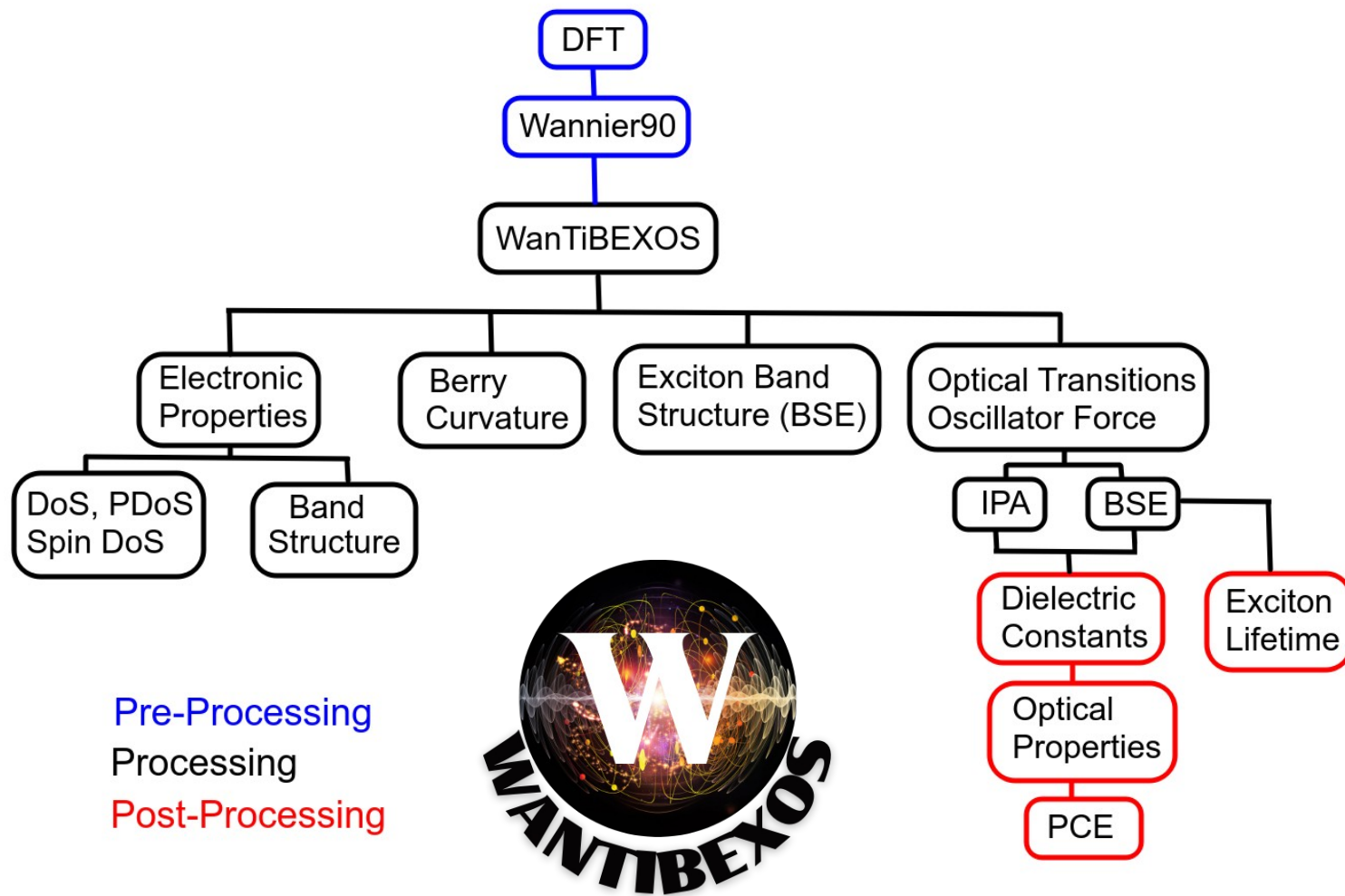


Prof. Dr. Adriano de  
Souza Martins  
DF/UFF

## Software Installation

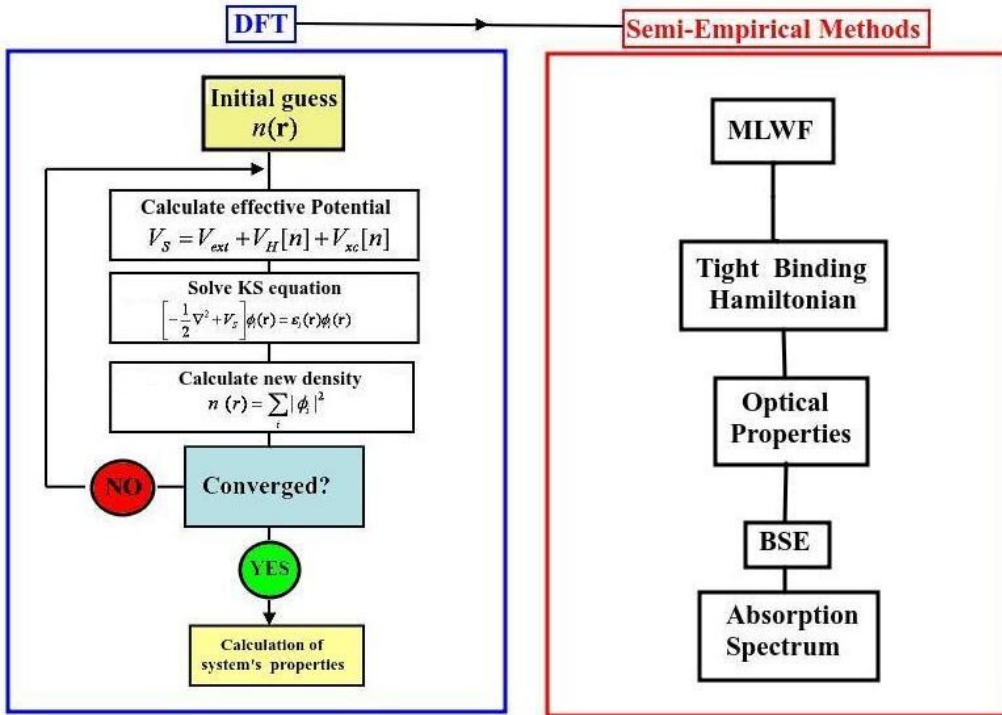
- Call Intel fortran compiler
- Download the code: git clone -b dev <https://github.com/ac-dias/wantibexos.git>
- Enter in WanTiBEXOS folder
- Do the make all command
- All executables will be at ./bin folder
- User manual available at: <https://wantibexos.readthedocs.io/en/latest>
- Examples of this mini-course available at:  
<https://github.com/ac-dias/wantibexos-recipes>
- Main executable: wtb.x
- Convert Wannier90 Hamiltonian: param\_gen\_vasp.x and param\_gen.x
- Siesta Hamiltonian converter: siesta2wtb.py
- FHI-aims Hamiltonian converter: aims2wtb.py
- Extended Huckel Hamiltonian Converter: huckel2wtb.x
- Calculates absorbance from optical properties: absorbance.x
- Power Conversion Efficiency calculation: pce.x
- Estimates the number of conduction and valence bands for BSE: nc\_nv\_finder.x

# WanTiBEXOS - Workflow



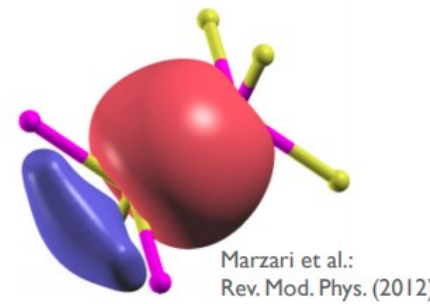
Pre-Processing  
Processing  
Post-Processing

# Wannier90



- Open-source code
- Interface with various DFT packages: VASP, Quantum Espresso, Siesta ...
- Calculates maximally localized Wannier functions
- Generates Tight Binding Hamiltonians that can be used in other applications
- Visualizes Wannier functions

W90



DOI:10.1088/1361-648X/ab51ff  
Available at: [www.wannier.org](http://www.wannier.org)

## MLWF-TB Hamiltonian Format

(Atom-centered WF)

<b>\$ less GaAs-WANN_hr.dat</b>				<b>Matrix element (eV)</b> $\langle s_1   H   s_1 \rangle = E_{s1}$
...	0 0 0	1	$\langle s_1  $	0.000000 Im part = 0
Home unit cell	0 0 0	2	$ s_1\rangle$	
0 0 0	3	1	-4.335108	
0 0 0	4	1	-0.000001	
0 0 0	5	1	0.000000	
0 0 0	6	1	-0.000001	
0 0 0	7	1	-1.472358	<b>Matrix element (eV)</b> $\langle s_2   H   s_1 \rangle = V_{ss\sigma}$
0 0 0	8	1	-1.157088	
...		1	-1.157088	
0 0	1	1	-1.157088	
...		1	-0.001219	$\langle p_2   H   s_1 \rangle = V_{sp}$
Neighbour unit cell				
				WF are well localized ⇒ nearest-neighbour suffice

# MLWF-TB Hamiltonian Format

```
1 |SOC
2   0.00          !scissors operator
3   -0.0          !efermi
4     3.1321841    0.0000000    0.0000000
5     -1.5660921   2.7125510    0.0000000
6     0.0000000    0.0000000   16.0000000
7 written on 4Sep2020 at 08:46:41
8           22
9           147
10      1   1   1   1   1   2   1   1   1   1   1   2   1   1   1   1
11      1   1   1   1   1   1   1   1   1   1   1   1   1   1   1   1
12      1   1   1   1   1   1   1   1   1   1   1   1   1   1   1   1
13      1   1   1   1   1   1   1   1   1   1   1   1   1   1   1   1
14      1   1   1   1   1   1   1   2   1   1   1   1   1   1   1   1
15      1   1   1   1   2   1   1   1   1   1   1   1   1   1   1   1
16      1   1   1   1   1   1   1   1   1   1   1   1   1   1   1   1
17      1   1   1   1   1   1   1   1   1   1   1   1   1   1   1   1
18      1   1   1   1   1   1   1   1   1   1   1   1   1   1   1   1
19      2   1   1   1   1   1   2   1   1   1   1   1   1   1   1   1
20     -8   -4   0   1   1   0.000065  -0.000000
21     -8   -4   0   2   1   -0.000000  -0.000000
22     -8   -4   0   3   1   0.000000  0.000000
23     -8   -4   0   4   1   -0.000002  0.000000
24     -8   -4   0   5   1   -0.000000  -0.000001
25     -8   -4   0   6   1   0.000016  -0.000000
26     -8   -4   0   7   1   0.000026  0.000000
27     -8   -4   0   8   1   -0.000009  0.000001
28     -8   -4   0   9   1   -0.000016  0.000000
29     -8   -4   0  10   1   0.000025  0.000000
30     -8   -4   0  11   1   -0.000010  0.000001
31     -8   -4   0  12   1   0.000001  0.000001
32     -8   -4   0  13   1   -0.000000  0.000000
33     -8   -4   0  14   1   0.000000  -0.000001
34     -8   -4   0  15   1   0.000000  0.000000
35     -8   -4   0  16   1   -0.000000  0.000000
```

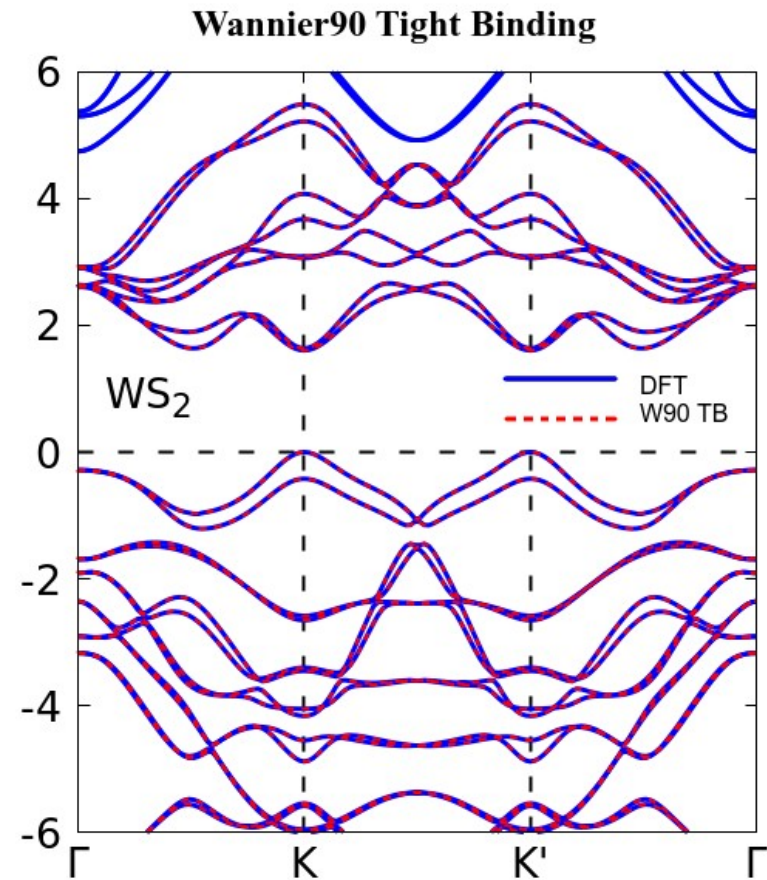
# Localized Basis Hamiltonian Format

```
1 NP
2 0.00000
3 -5.24385019
4 5.36610648 0.00000000 -0.00000000
5 -0.00000000 3.56638503 0.00000000
6 0.00000000 0.00000000 20.00000000
7 266
8 49
9 #rcell x  rcell y  rcell z  i  j  ReH  ImH  S
10 0.00000000 0.00000000 0.00000000 1  1  -4937.04316865 0.00000000 0.99999929
11 0.00000000 0.00000000 0.00000000 1  2  0.07195103 0.00000000 -0.00000021
12 0.00000000 0.00000000 0.00000000 1  3  -0.21887571 -0.00000000 -0.00000008
13 0.00000000 0.00000000 0.00000000 1  4  -0.10984543 -0.00000000 -0.00000003
14 0.00000000 0.00000000 0.00000000 1  5  0.10576113 -0.00000000 0.00000003
15 0.00000000 0.00000000 0.00000000 1  6  0.00006136 -0.00000000 0.00000000
16 0.00000000 0.00000000 0.00000000 1  7  0.00159698 -0.00000000 0.00000000
17 0.00000000 0.00000000 0.00000000 1  8  0.00000215 0.00000000 0.00000000
18 0.00000000 0.00000000 0.00000000 1  9  0.00002365 -0.00000000 0.00000000
19 0.00000000 0.00000000 0.00000000 1  10 0.00076499 0.00000000 0.00000000
20 0.00000000 0.00000000 0.00000000 1  11 -0.00000097 0.00000000 0.00000000
21 0.00000000 0.00000000 0.00000000 1  12 0.00000730 -0.00000000 0.00000000
22 0.00000000 0.00000000 0.00000000 1  13 0.00026677 0.00000000 0.00000000
23 0.00000000 0.00000000 0.00000000 1  14 -0.00000004 0.00000000 0.00000000
24 0.00000000 0.00000000 0.00000000 1  15 -0.00000001 0.00000000 0.00000000
25 0.00000000 0.00000000 0.00000000 1  16 0.00000003 0.00000000 0.00000000
26 0.00000000 0.00000000 0.00000000 1  17 -0.00027474 -0.00000000 -0.00000000
27 0.00000000 0.00000000 0.00000000 1  18 -0.00000070 -0.00000000 0.00000000
28 0.00000000 0.00000000 0.00000000 1  19 0.00038001 -0.00000000 -0.00000000
29 0.00000000 0.00000000 0.00000000 1  20 0.00000000 0.00000000 0.00000000
30 0.00000000 0.00000000 0.00000000 1  21 -0.00000039 0.00000000 0.00000000
31 0.00000000 0.00000000 0.00000000 1  22 0.00020662 0.00000000 0.00000000
32 0.00000000 0.00000000 0.00000000 1  23 0.00000057 0.00000000 0.00000000
33 0.00000000 0.00000000 0.00000000 1  24 -0.00021482 -0.00000000 0.00000000
34 0.00000000 0.00000000 0.00000000 1  25 -0.00000031 -0.00000000 0.00000000
35 0.00000000 0.00000000 0.00000000 1  26 0.00000004 -0.00000000 0.00000000
```

# MLWF-TB Hamiltonian Characteristics

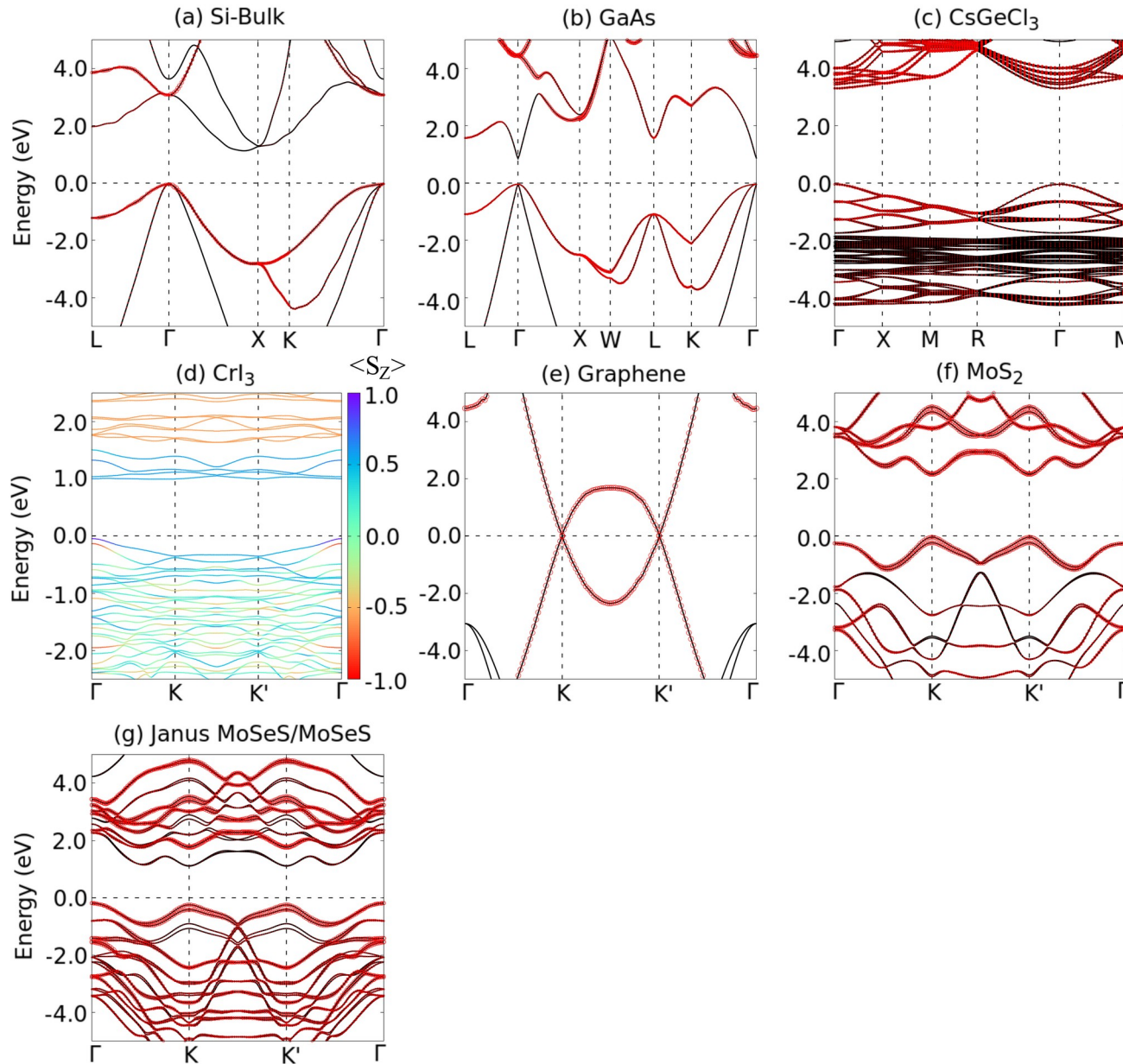
$$H(\mathbf{k}) = H_0 + \sum_{i=1}^N e^{i\mathbf{k}\cdot\mathbf{R}_i} H_{\mathbf{R}_i}$$

- Orthogonal basis set
- Large parameter set
- Matrix elements directly derived from DFT
- Model accounts for multiple neighboring unit cells
- Fixed bond length model
- Non-transferable parameters
- High-precision model

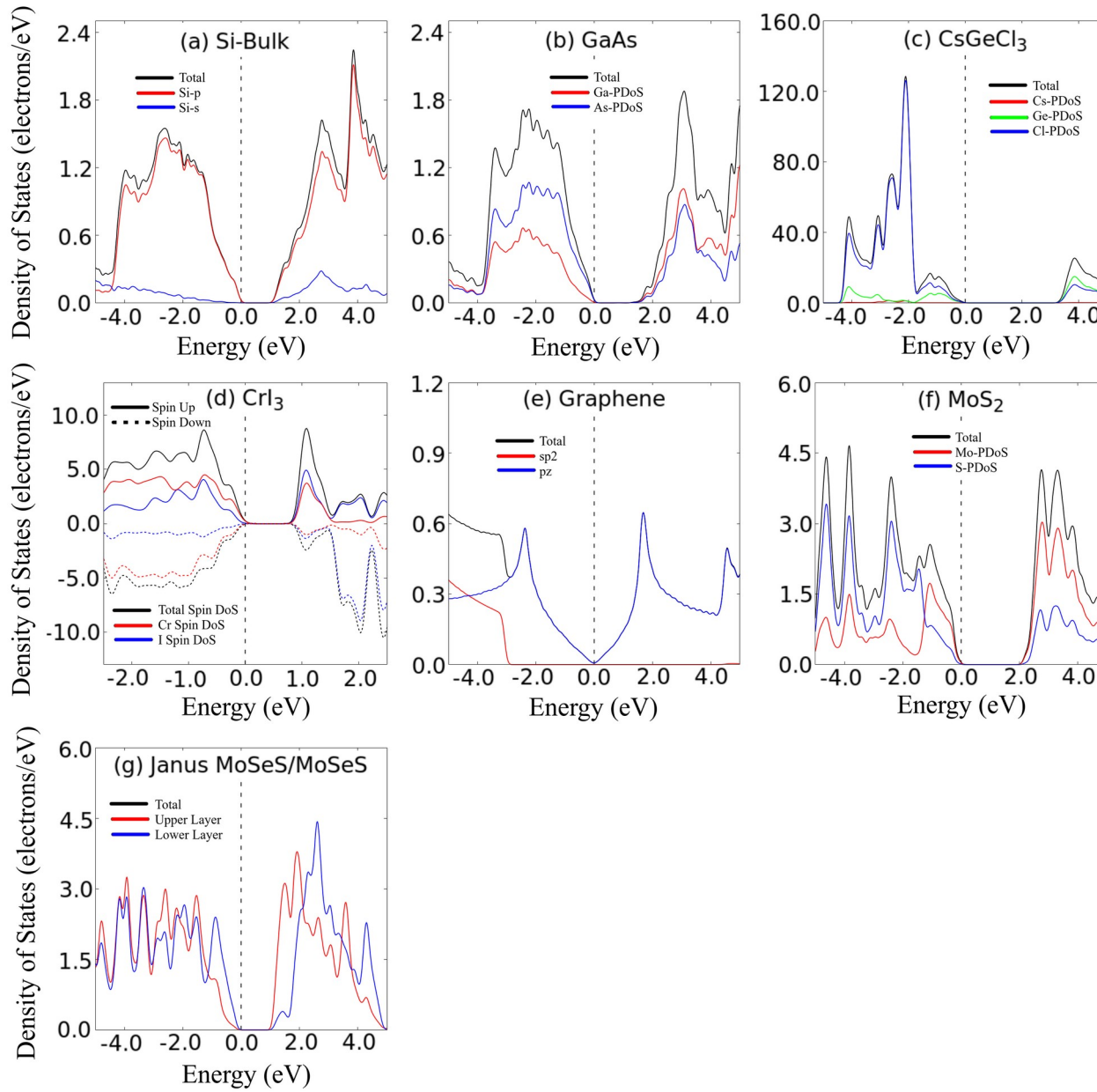


DOI: 10.1016/j.cpc.2007.11.016  
(Wannier90 paper)

# Electronic Band Structure



# Density of States



# Thermoelectric Properties (CRTA)

Transport Distribution Function

$$\Sigma_{i,j}(E) = \frac{1}{VN_k} \sum_{n,k} v_i(n, k) v_j(n, k) \tau_{n,k} \delta(E - E_{n,k})$$

In CRTA the lifetime assumes one value for all electrons and other value for all holes.

Electron Conductivity

$$\sigma_{i,j}(\mu, T) = e^2 \int dE \left( -\frac{\partial f(E, \mu, T)}{\partial E} \right) \Sigma_{i,j}(E)$$

Figure of Merit

$$ZT = \frac{\sigma^2 S^2 T}{\kappa + \kappa_l}$$

Seebeck Coefficient

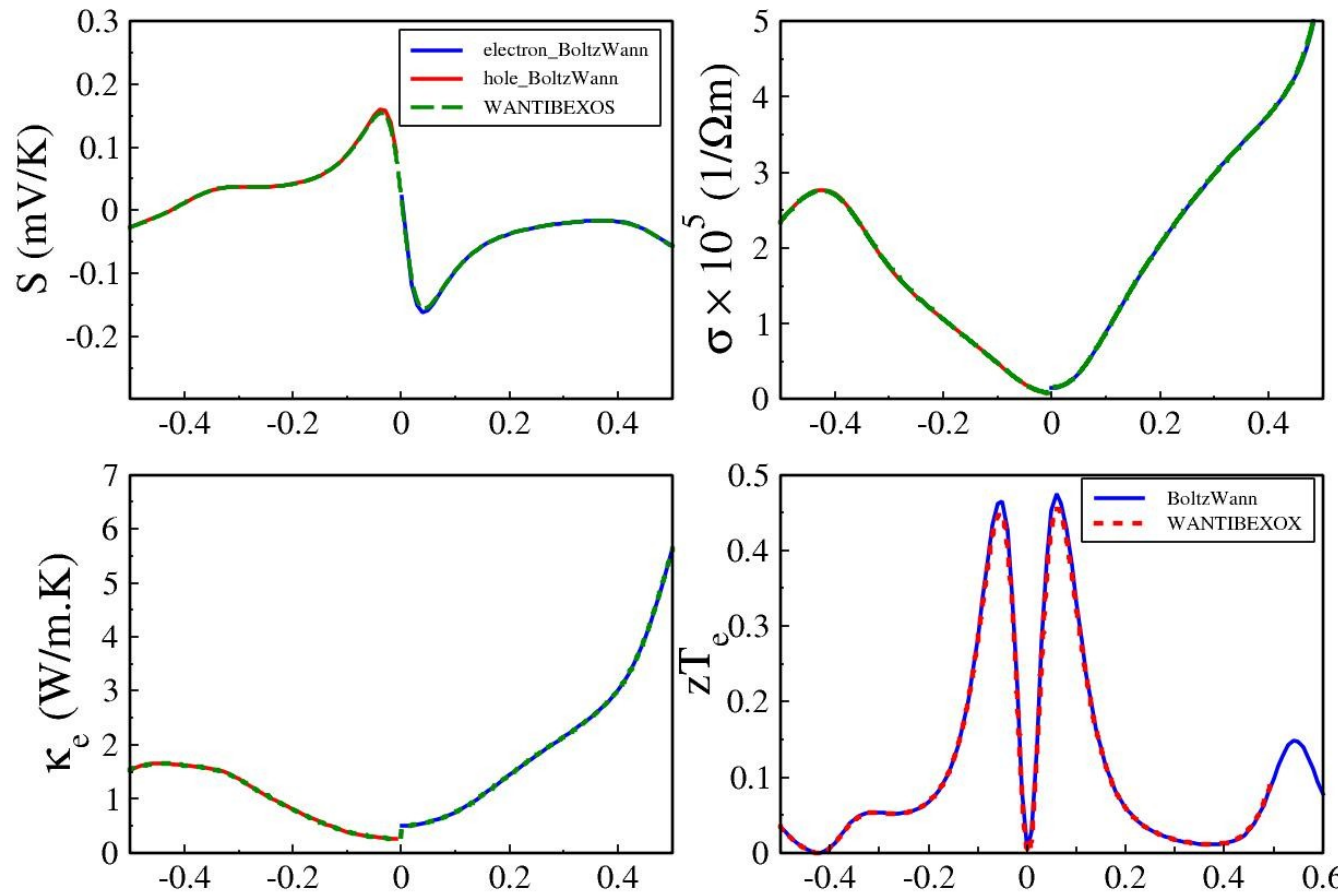
$$S_{i,j}(\mu, T) = \frac{e}{T \sigma_{i,j}(\mu, T)} \int dE \left( -\frac{\partial f(E, \mu, T)}{\partial E} \right) (E - \mu) \Sigma_{i,j}(E)$$

Electron Thermal Conductivity

$$\kappa_{i,j}(\mu, T) = \frac{1}{T} \int dE \left( -\frac{\partial f(E, \mu, T)}{\partial E} \right) (E - \mu)^2 \Sigma_{i,j}(E)$$

# Thermoelectric Properties (CRTA)

AsO T=300K



# Effective Mass Tensor

Effective mass definition

$$\left( \frac{1}{m^*} \right)_{ij} = \frac{1}{\hbar^2} \frac{\partial^2 E_n(\vec{k})}{\partial k_i \partial k_j}$$

Effective mass tensor

$$\frac{d^2 E}{dk^2} = \begin{pmatrix} \frac{d^2 E}{dk_x^2} & \frac{d^2 E}{dk_x dk_y} & \frac{d^2 E}{dk_x dk_z} \\ \frac{d^2 E}{dk_y dk_x} & \frac{d^2 E}{dk_y^2} & \frac{d^2 E}{dk_y dk_z} \\ \frac{d^2 E}{dk_z dk_x} & \frac{d^2 E}{dk_z dk_y} & \frac{d^2 E}{dk_z^2} \end{pmatrix}$$

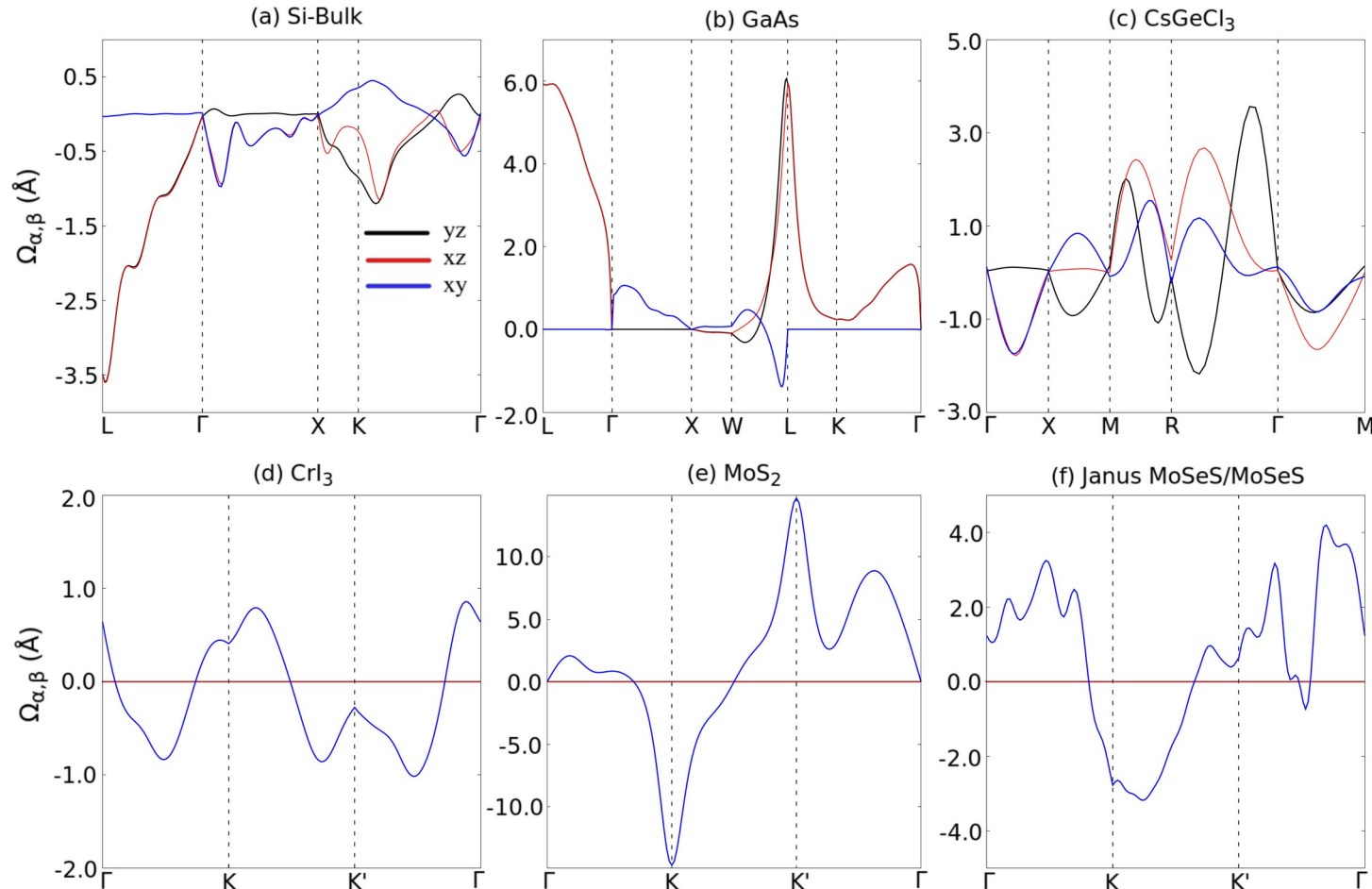
Numerical evaluation of the second derivatives

$$\frac{\partial^2 f}{\partial x^2} \approx \frac{1}{12h^2} \begin{pmatrix} -(f_{-2} + f_2) \\ 16(f_{-1} + f_1) \\ -30(f) \end{pmatrix},$$

$$\frac{\partial^2 f}{\partial x \partial y} \approx \frac{1}{600h^2} \begin{pmatrix} -63(f_{1,-2} + f_{2,-1} + f_{-2,1} + f_{-1,2}) + \\ 63(f_{-1,-2} + f_{-2,-1} + f_{1,2} + f_{2,1}) + \\ 44(f_{2,-2} + f_{-2,2} - f_{-2,-2} - f_{2,2}) + \\ 74(f_{-1,-1} + f_{1,1} - f_{1,-1} - f_{-1,1}) \end{pmatrix}.$$

# Berry Curvature

$$\Omega_{\alpha,\beta}(\mathbf{k}) = -2\text{Im} \sum_{v,c} \frac{\langle c, \mathbf{k} | P_\alpha | v, \mathbf{k} \rangle \langle v, \mathbf{k} | P_\beta | c, \mathbf{k} \rangle}{(E_{c,\mathbf{k}} - E_{v,\mathbf{k}})^2} . \quad P_\alpha = \frac{\partial H(\mathbf{k})}{\partial k_\alpha} ,$$



## Optical Properties

### Dielectric Tensor

$$\epsilon_{1,\alpha,\beta}(\omega) = \delta_{\alpha,\beta} + \frac{e^2 S_p}{\epsilon_0 \Omega N_{\mathbf{k}}} \sum_{\mathbf{k},c,v} F_{\alpha,\beta}^{c,v,\mathbf{k}} \frac{(E_{c,\mathbf{k}} - E_{v,\mathbf{k}}) - \hbar\omega}{(\hbar\omega - (E_{c,\mathbf{k}} - E_{v,\mathbf{k}}))^2 + \eta^2} ,$$

$$\epsilon_{2,\alpha,\beta}(\omega) = \frac{e^2 S_p}{\epsilon_0 \Omega N_{\mathbf{k}}} \sum_{\mathbf{k},c,v} F_{\alpha,\beta}^{c,v,\mathbf{k}} \frac{\eta}{(\hbar\omega - (E_{c,\mathbf{k}} - E_{v,\mathbf{k}}))^2 + \eta^2} ,$$

### Oscillator Force (IPA)

$$F_{\alpha,\beta}^{c,v,\mathbf{k}} = \frac{\langle c, \mathbf{k} | P_\alpha | v, \mathbf{k} \rangle \langle v, \mathbf{k} | P_\beta | c, \mathbf{k} \rangle}{(E_{c,\mathbf{k}} - E_{v,\mathbf{k}} - i\eta_1)(E_{c,\mathbf{k}} - E_{v,\mathbf{k}} + i\eta_1)} ,$$

$$P_\alpha = \frac{\partial H(\mathbf{k})}{\partial k_\alpha} , \quad \alpha = x, y, z$$

# Optical Properties

Extinction Coefficient

$$\kappa_{\alpha,\beta}(\omega) = \left[ \frac{\sqrt{\epsilon_{1,\alpha,\beta}^2(\omega) + \epsilon_{2,\alpha,\beta}^2(\omega)} - \epsilon_{1,\alpha,\beta}(\omega)}{2} \right]^{\frac{1}{2}}$$

Refractive Index

$$n_{\alpha,\beta}(\omega) = \left[ \frac{\sqrt{\epsilon_{1,\alpha,\beta}^2(\omega) + \epsilon_{2,\alpha,\beta}^2(\omega)} + \epsilon_{1,\alpha,\beta}(\omega)}{2} \right]^{\frac{1}{2}}$$

Absorption Coefficient

$$A_{\alpha,\beta}(\omega) = \frac{\sqrt{2}\omega}{c} \left[ \sqrt{\epsilon_{1,\alpha,\beta}^2(\omega) + \epsilon_{2,\alpha,\beta}^2(\omega)} - \epsilon_{1,\alpha,\beta}(\omega) \right]^{\frac{1}{2}}.$$

PL emission Intensity

$$I_{\alpha}^{PL}(\omega) = Im \sum_{c,v,k} \frac{|F_{\alpha,\alpha}^{c,v,k}|^2}{\pi^2 \hbar c^3 N_k} \left[ \omega^3 n_{\alpha,\alpha}(\omega) \frac{1}{\omega - (E_{c,k} - E_{v,k}) + i\eta} e^{-\frac{(E_{c,k} - E_{v,k}) - E_{min}}{k_B T_{exc}}} \right]$$

Energy Loss Function

$$L_{\alpha,\beta}(\omega) = \frac{\epsilon_{2,\alpha,\beta}}{\epsilon_{1,\alpha,\beta}^2 + \epsilon_{2,\alpha,\beta}^2}.$$

Reflectivity

$$R_{\alpha,\beta}(\omega) = \frac{(n_{\alpha,\beta}(\omega) - 1)^2 + \kappa_{\alpha,\beta}^2(\omega)}{(n_{\alpha,\beta}(\omega) + 1)^2 + \kappa_{\alpha,\beta}^2(\omega)}$$

# BSE Formalism for Orthogonal Basis Hamiltonian

Exciton Hamiltonian

$$H_{exc} = H_e + H_h + V_{eh} ,$$

TDA Exciton wave-function

$$\Psi_{ex}^n(\mathbf{Q}) = \sum_{c,v,\mathbf{k}} A_{c,v,\mathbf{k},\mathbf{Q}}^n (|c, \mathbf{k} + \mathbf{Q}\rangle \otimes |v, \mathbf{k}\rangle) ,$$

Bethe-Salpeter Equation in exciton subspace (TDA)

$$(E_{c,\mathbf{k}+\mathbf{Q}} - E_{v,\mathbf{k}}) A_{c,v,\mathbf{k},\mathbf{Q}}^n + \frac{1}{\Omega N_k} \sum_{\mathbf{k}',v',c'} W_{(\mathbf{k},v,c),(\mathbf{k}',v',c'),\mathbf{Q}} A_{c',v',\mathbf{k}',\mathbf{Q}}^n = E_{\mathbf{Q}}^n A_{c,v,\mathbf{k},\mathbf{Q}}^n ,$$

where

$$W_{(\mathbf{k},v,c),(\mathbf{k}',v',c'),\mathbf{Q}} =$$

$$W_{(\mathbf{k},v,c),(\mathbf{k}',v',c'),\mathbf{Q}}^d + W_{(\mathbf{k},v,c),(\mathbf{k}',v',c'),\mathbf{Q}}^x .$$

and

$$W_{(\mathbf{k},v,c),(\mathbf{k}',v',c'),\mathbf{Q}}^d = V(\mathbf{k} - \mathbf{k}')$$

$$\times \langle c, \mathbf{k} + \mathbf{Q} | c', \mathbf{k}' + \mathbf{Q} \rangle \langle v', \mathbf{k}' | v, \mathbf{k} \rangle$$

$$W_{(\mathbf{k},v,c),(\mathbf{k}',v',c'),\mathbf{Q}}^x = -V(\mathbf{Q})$$

$$\times \langle c, \mathbf{k} + \mathbf{Q} | v, \mathbf{k} \rangle \langle v', \mathbf{k}' | c', \mathbf{k}' + \mathbf{Q} \rangle .$$

# BSE Formalism for Orthogonal Basis Hamiltonian

Coulomb potential options to model Electron-hole interaction

1) Bare Coulomb Potential

$$V(\mathbf{Q}) = -\frac{e^2}{2V_{uc}\epsilon_0\epsilon_d\mathbf{Q}^2} ,$$

2) 2D Keldysh Potential

$$V(\mathbf{Q}) = -\frac{e^2}{2A_{uc}\epsilon_0\epsilon_d|\mathbf{Q}|(1 + r_0|\mathbf{Q}|)} .$$

3) 2D Rytova-Keldysh Potential

$$V(\mathbf{Q}) = -\frac{e^2}{2A_{uc}\epsilon_0|\mathbf{Q}|F(\mathbf{Q})} e^{-w_0|\mathbf{Q}|} ,$$

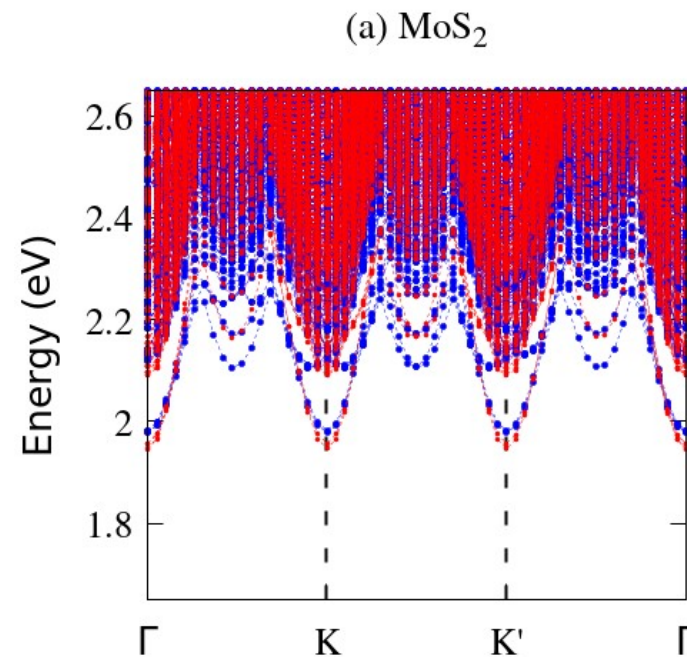
$$F(\mathbf{Q}) = \frac{\left[1 - (p_b p_t e^{-2|\mathbf{Q}|\eta l_c})\right] \kappa}{\left[1 - (p_t e^{-\eta|\mathbf{Q}|l_c})\right] \left[1 - (p_b e^{-\eta|\mathbf{Q}|l_c})\right]} + r_0|\mathbf{Q}|e^{-w_0|\mathbf{Q}|}$$

4) 2D Coulomb Truncated Potential

$$V(\mathbf{Q}) = -\frac{e^2}{2V_{uc}\epsilon_0\mathbf{Q}^2} \times [1 - e^{-C_2} (C_1 \sin(C_3) - \cos(C_3))] ,$$

$$C_1 = \frac{|Q_z|}{\sqrt{Q_x^2 + Q_y^2}} , \quad C_2 = \frac{\mathbf{r}_3}{2} \sqrt{Q_x^2 + Q_y^2} ,$$

$$C_3 = \frac{\mathbf{r}_3}{2} |Q_z| .$$



# BSE Formalism for Orthogonal Basis Hamiltonian

5) Simplified 2D Coulomb Truncated Potential

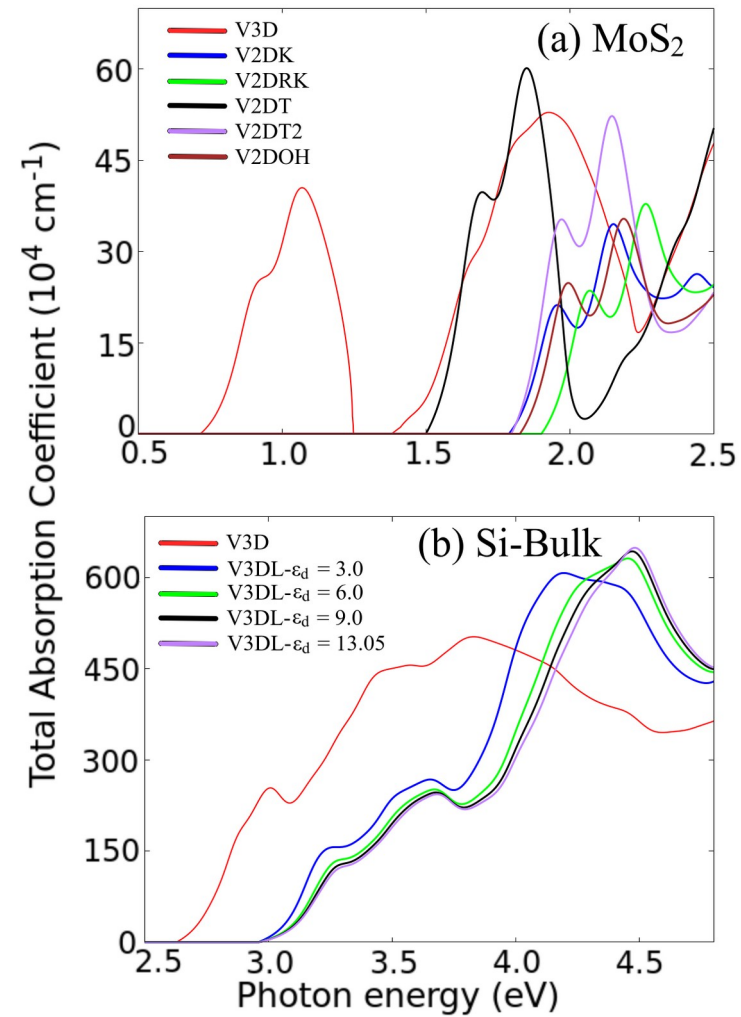
$$V(\mathbf{Q}) = -\frac{e^2}{2V_{uc}\epsilon_0 \mathbf{Q}^2} \times [1 - e^{-Q_{xy}Z_c} \cos(Q_z Z_c)] ,$$

6) 2D Ohno Potential

$$V(\mathbf{Q}) = -\frac{e^2}{2A_{uc}\epsilon_0\epsilon_d |\mathbf{Q}|} e^{-w_0|\mathbf{Q}|} ,$$

7) 0D Potential

$$V(\mathbf{Q}) = -\frac{e^2}{2V_{uc}\epsilon_0 \mathbf{Q}^2} [1 - \cos(0.5r_{min}|\mathbf{Q}|)]$$



## Optical Properties at BSE formalism

### Dielectric Functions with Excitonic Effects

$$\epsilon_{1,\alpha,\beta}^{BSE}(\omega) = \delta_{\alpha,\beta} + \frac{e^2 S_p}{\epsilon_0 \Omega N_k} \sum_n F_{\alpha,\beta}^{n,BSE} \frac{E_0^n - \hbar\omega}{(\hbar\omega - E_0^n)^2 + \eta^2} ,$$

$$\epsilon_{2,\alpha,\beta}^{BSE}(\omega) = \frac{e^2 S_p}{\epsilon_0 \Omega N_k} \sum_n F_{\alpha,\beta}^{n,BSE} \frac{\eta}{(\hbar\omega - E_0^n)^2 + \eta^2}$$

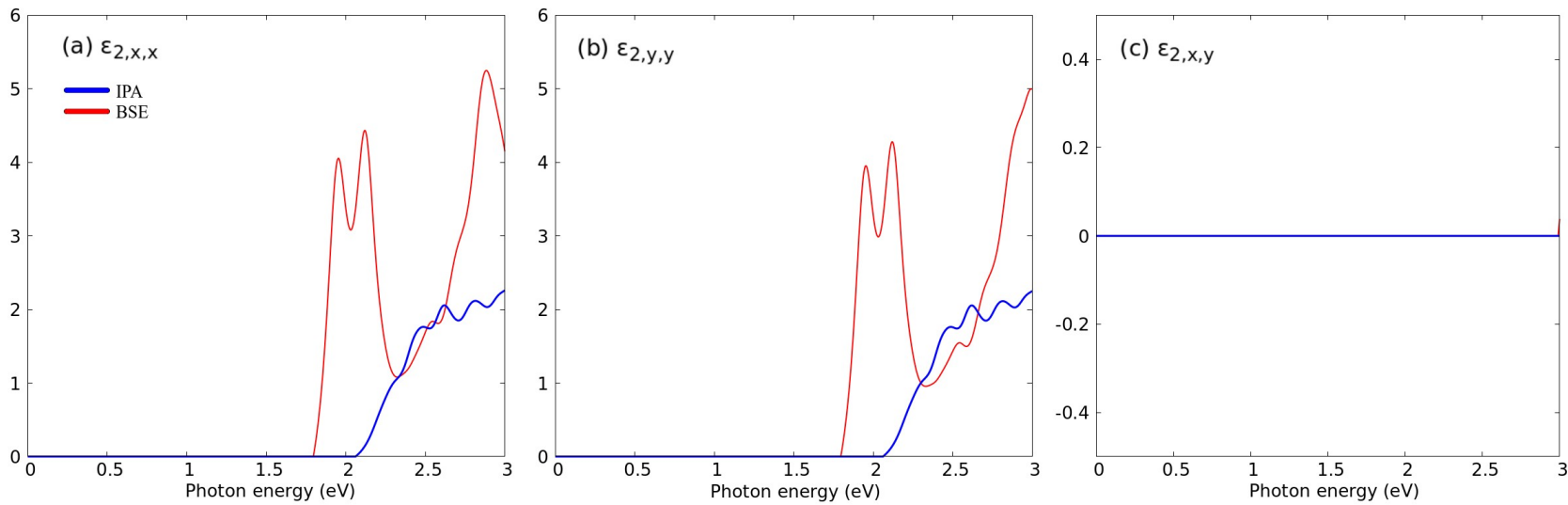
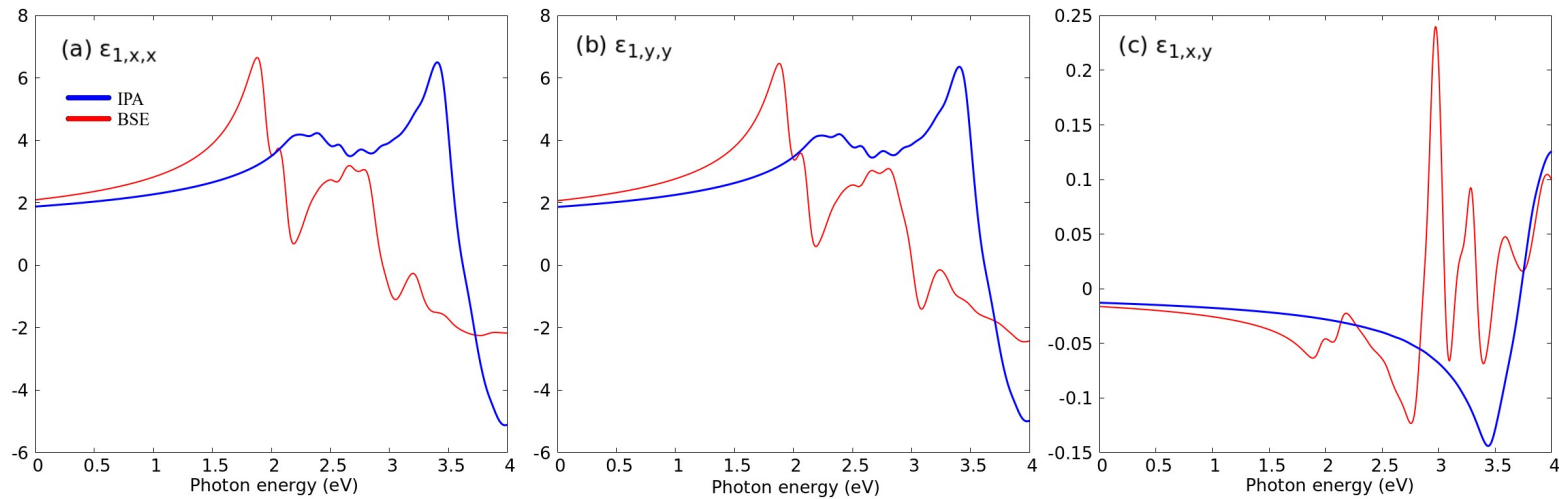
### Oscillator Force (BSE)

$$F_{\alpha,\beta}^{n,BSE} = \left( \sum_{c,v,\mathbf{k}} \frac{A_{c,v,\mathbf{k},0}^n \langle c, \mathbf{k} | P_\alpha | v, \mathbf{k} \rangle}{(E_{c,\mathbf{k}} - E_{v,\mathbf{k}} + i\eta_1)} \right) \left( \sum_{c',v',\mathbf{k}'} \frac{A_{c',v',\mathbf{k}',0}^{n*} \langle v', \mathbf{k}' | P_\beta | c', \mathbf{k}' \rangle}{(E_{c',\mathbf{k}'} - E_{v',\mathbf{k}'} - i\eta_1)} \right)$$

### PL emission Intensity (BSE)

$$I_\alpha^{PL}(\omega) = Im \sum_n \frac{|F_{\alpha,\alpha}^{n,BSE}|^2}{\pi^2 \hbar c^3 N_k} \left[ \omega^3 n_{\alpha,\alpha}(\omega) \frac{1}{\omega - E_n + i\eta} e^{-\frac{E_n - E_{min}}{k_B T_{exc}}} \right]$$

# Optical Properties at BSE formalism



# BSE Formalism with Temperature Effects

$$\begin{aligned}
 & (E_{c,\mathbf{k}+\mathbf{Q}}^\Delta - E_{v,\mathbf{k}}) A_{c,v,\mathbf{k},\mathbf{Q}}^n \\
 & + \frac{(f(E_{v,\mathbf{k}}) - f(E_{c,\mathbf{k}+\mathbf{Q}}^\Delta))}{N_k} \\
 & \times \sum_{\mathbf{k}',v',c'} W_{(\mathbf{k},v,c),(\mathbf{k}',v',c'),\mathbf{Q}} A_{c',v',\mathbf{k}',\mathbf{Q}}^n \\
 & = E_{\mathbf{Q}}^n A_{c,v,\mathbf{k},\mathbf{Q}}^n ,
 \end{aligned}$$

where

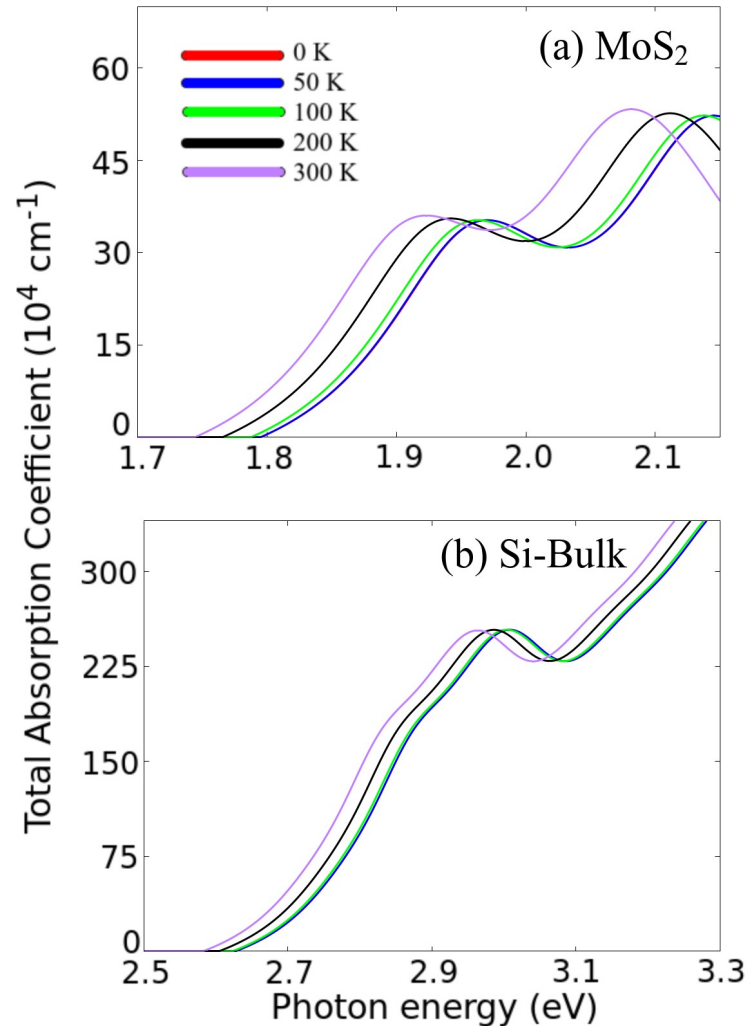
$$E_{c,\mathbf{k}+\mathbf{Q}}^\Delta = E_{c,\mathbf{k}+\mathbf{Q}} - \Delta(\alpha_B, \Theta, T) ,$$

Empirical Band Gap correction

$$\Delta(\alpha_B, \Theta, T) = \frac{2\alpha_B}{e^{\Theta/T} - 1} ,$$

or

$$\Delta(\alpha_B, \Theta, T) = \alpha_B \Theta \left[ \coth \left( \frac{\alpha_B}{2k_b T} \right) - 1 \right] ,$$



## Power Conversion Efficiency

$$\text{PCE} = \frac{P_{\text{PV}}}{P_{\text{solar}}} , \quad P_{\text{solar}} = \int_0^{\infty} P(E) dE ,$$

$$P_{\text{PV}} = J(V_{\max}) V_{\max} ,$$

$$J(V) = J_{sc} - \frac{J_0}{fr} \left( \exp \left( \frac{eV}{k_B T} \right) - 1 \right) ,$$

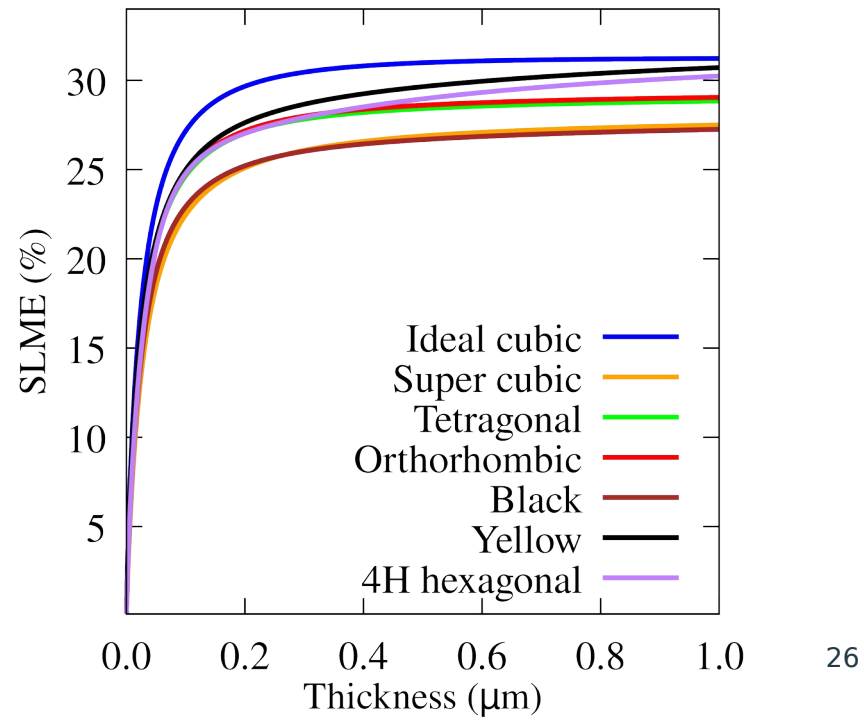
$$fr = e^{-\frac{\delta}{k_B T}}$$



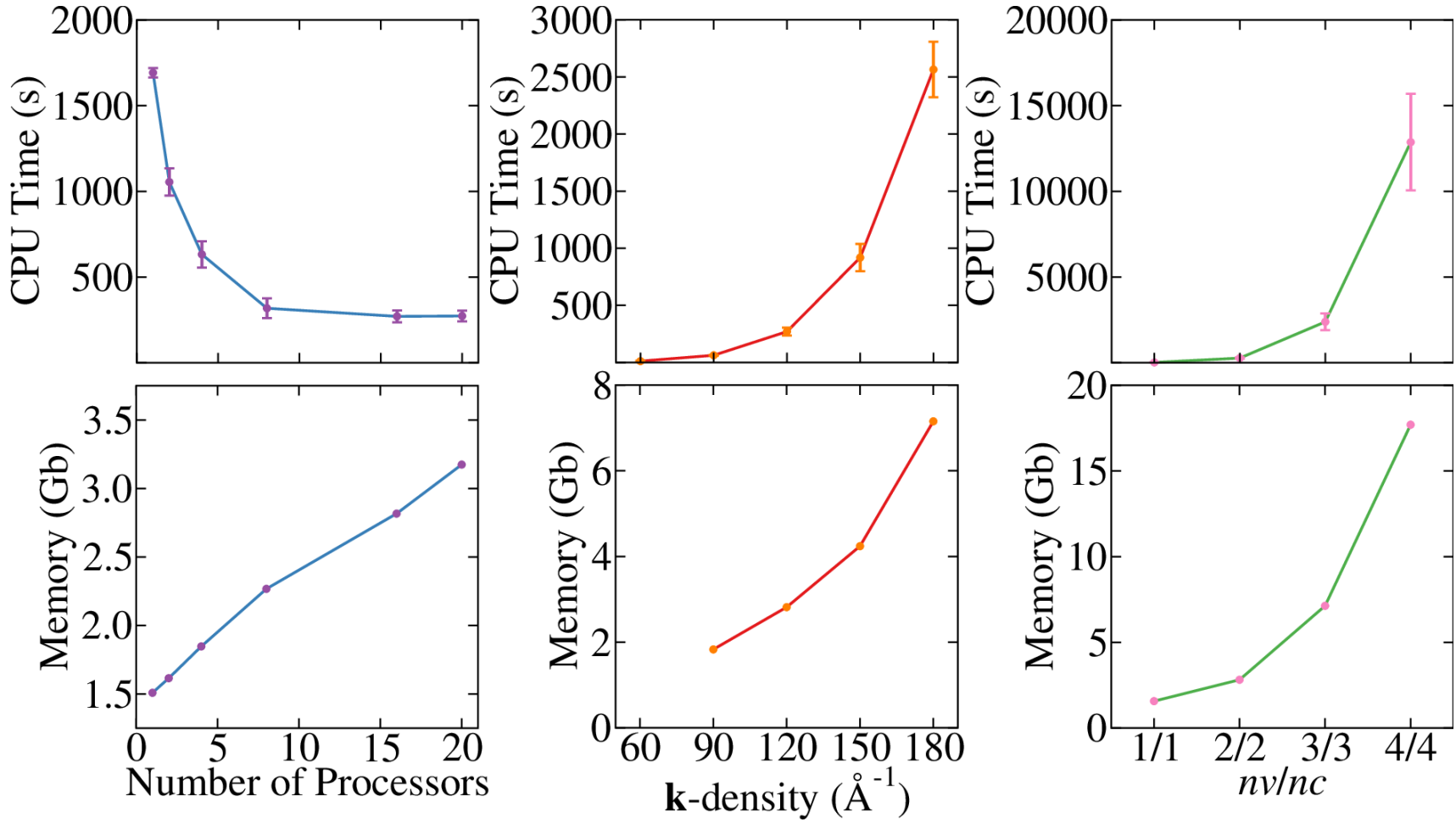
$$J_{sc} = e \int_0^{\infty} a(E) \frac{P(E)}{E} dE ,$$

$$J_0 = e\pi \int_0^{\infty} a(E) \Phi_{bb}(E) dE ,$$

$$\Phi_{bb}(E) = \frac{2E^2}{h^3 v_c^2} \left( e^{\frac{E}{k_B T}} - 1 \right)^{-1} ,$$



## Benchmark



# Hands-On

## Auxiliary Input Files

kpoints.dat

```
1 6
2 50
3   0.0000000000  0.0000000000  0.0000000000      GAMMA
4   0.6666666667 -0.3333333333  0.0000000000      K
5
6   0.6666666667 -0.3333333333  0.0000000000      K
7   0.3333333333  0.3333333333  0.0000000000      K'
8
9   0.3333333333  0.3333333333  0.0000000000      K'
10  0.0000000000  0.0000000000  0.0000000000      GAMMA
11
12
```

orbw.dat

```
1 1
2 1
3 1
4 1
5 1
6 0
7 0
8 0
9 0
10 0
11 0
12 1
13 1
14 1
15 1
16 1
17 0
18 0
19 0
20 0
21 0
22 0|
```

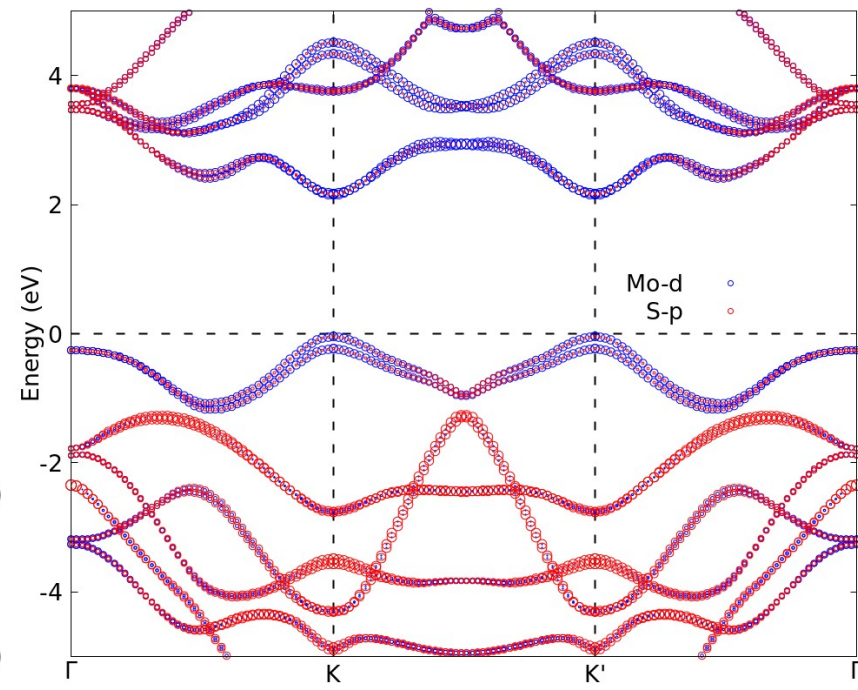
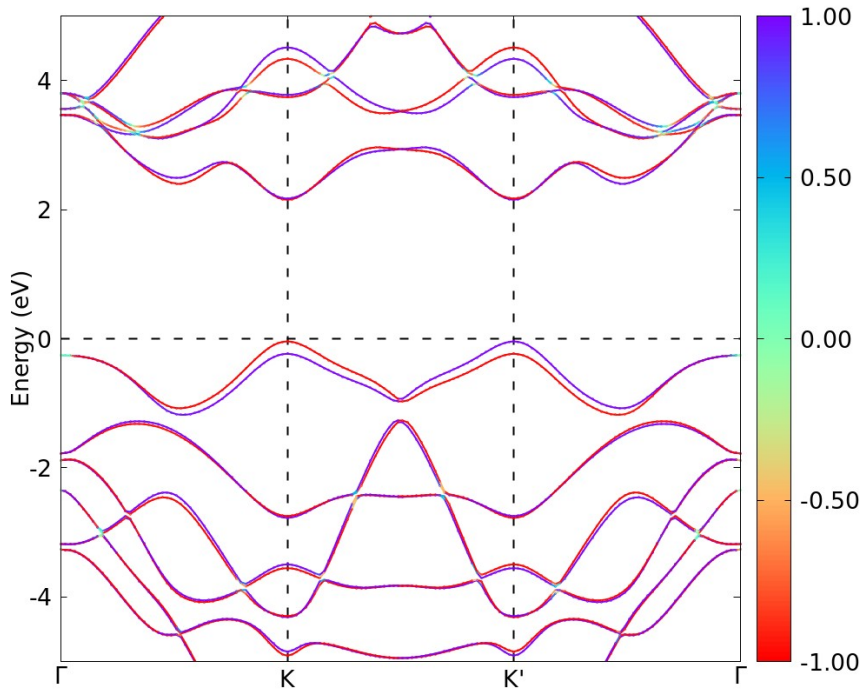
kpoints-bse.dat

```
1 6
2 15
3   0.0000000000  0.0000000000  0.0000000000      GAMMA
4   0.6666666667 -0.3333333333  0.0000000000      K
5
6   0.6666666667 -0.3333333333  0.0000000000      K
7   0.3333333333  0.3333333333  0.0000000000      K'
8
9   0.3333333333  0.3333333333  0.0000000000      K'
10  0.0000000000  0.0000000000  0.0000000000      GAMMA
11
```

## Hands-On : Band Structure

```
1 NTHREADS= 8
2 SYSDIM= "2D"
3 DFT= V
4
5 PARAMS_FILE= "tb_mos2.dat"
6 KPATH_FILE= "kpoints.dat"
7 KPATH_BSE= "kpoints-bse.dat"
8 OUTPUT= "./out/"
9 CALC_DATA= "./out/"
10
11 BANDS= T
12 ORB_W= "orb_w_s-p.dat"
13
```

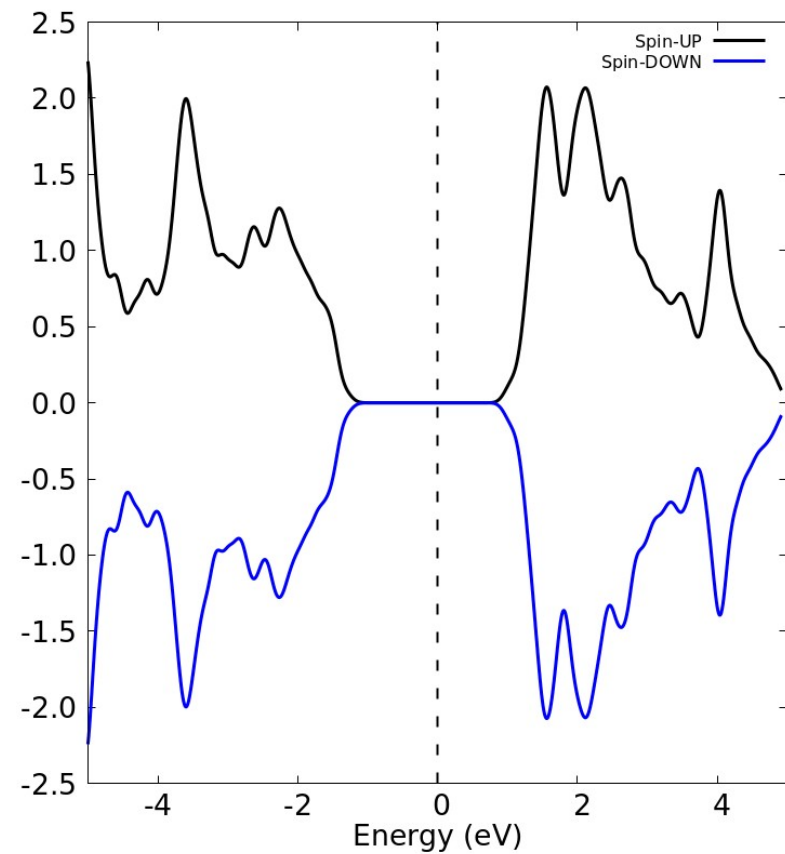
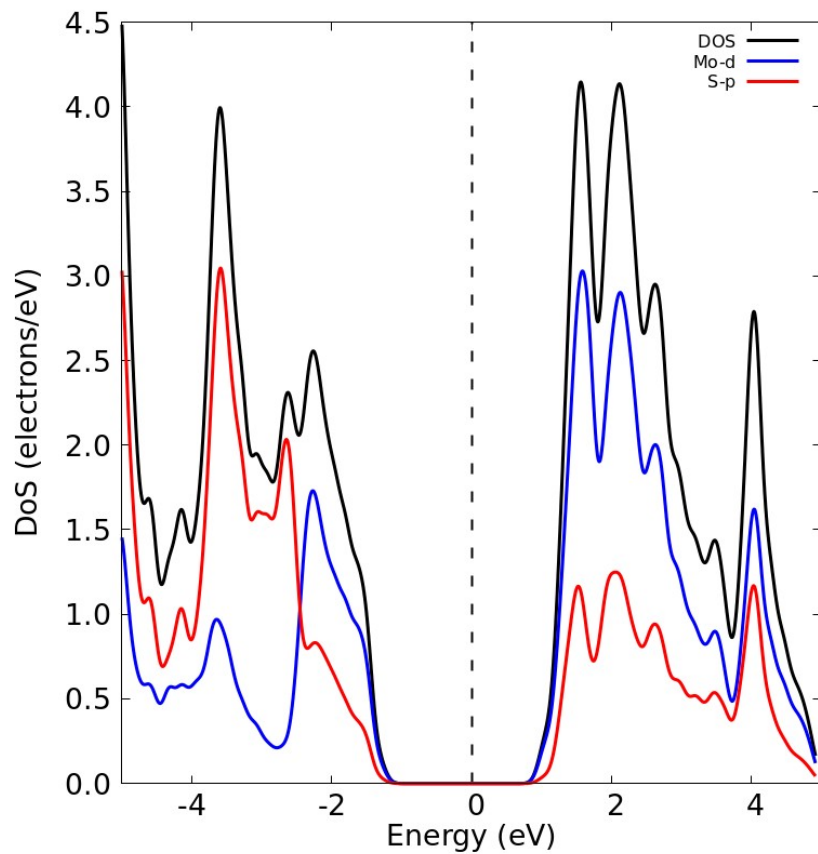
# Hands-On : Band Structure



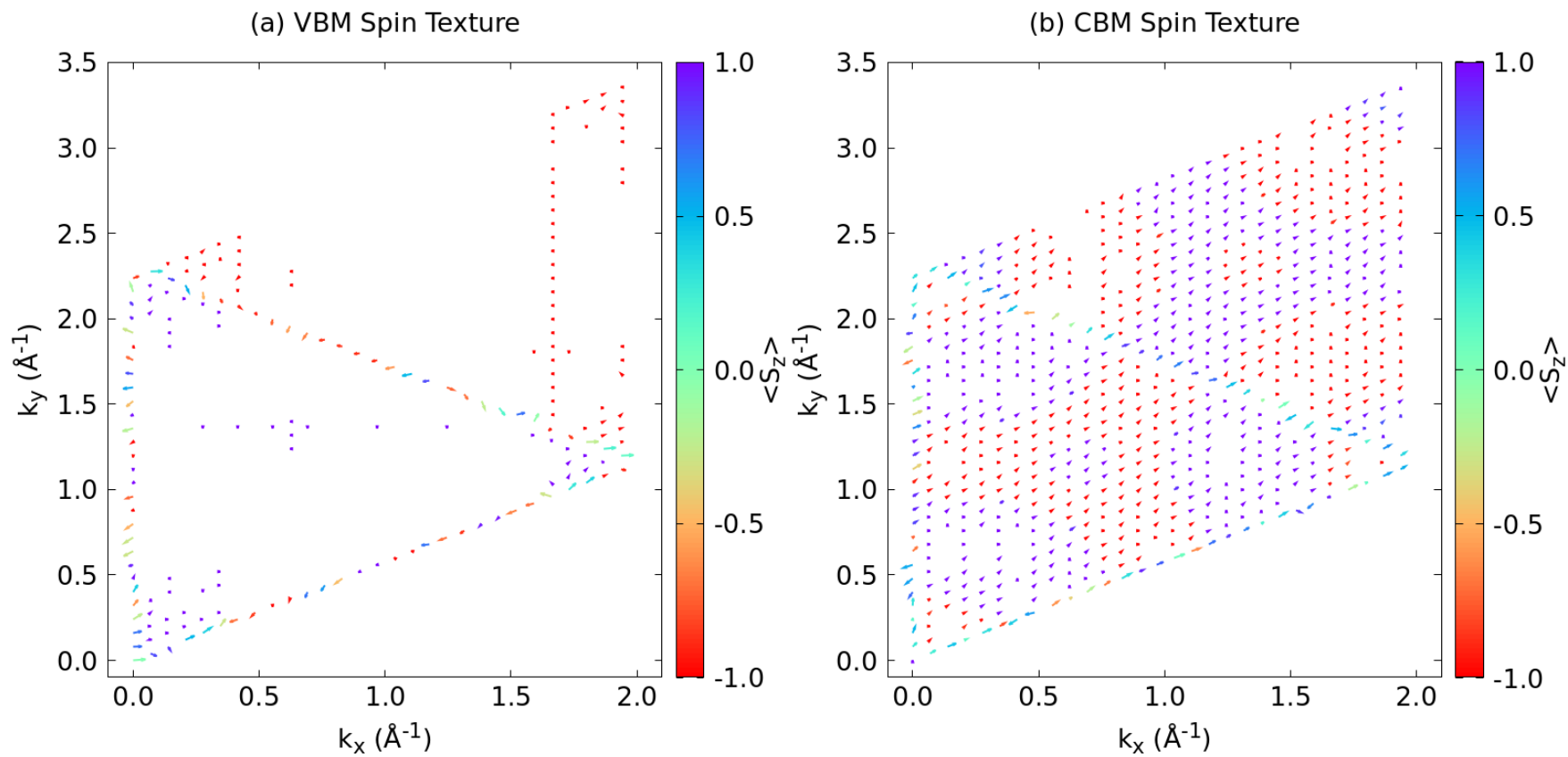
## Hands-On : Density of States

```
1 NTHREADS= 8
2 SYSDIM= "2D"
3 DFT= V
4
5 PARAMS_FILE= "tb_hr.dat"
6 KPATH_FILE= "kpoints.dat"
7 KPATH_BSE= "kpoints-bse.dat"
8 OUTPUT= "./out/"
9 CALC_DATA= "./out/"
10
11 MESH_TYPE= "RK2D"
12 RK= 80
13
14 DOS= T
15 ORB_W= "orb_w_s-p.dat"
16
17 SPIN_TXT= T
18
19
```

## Hands-On : Density of States



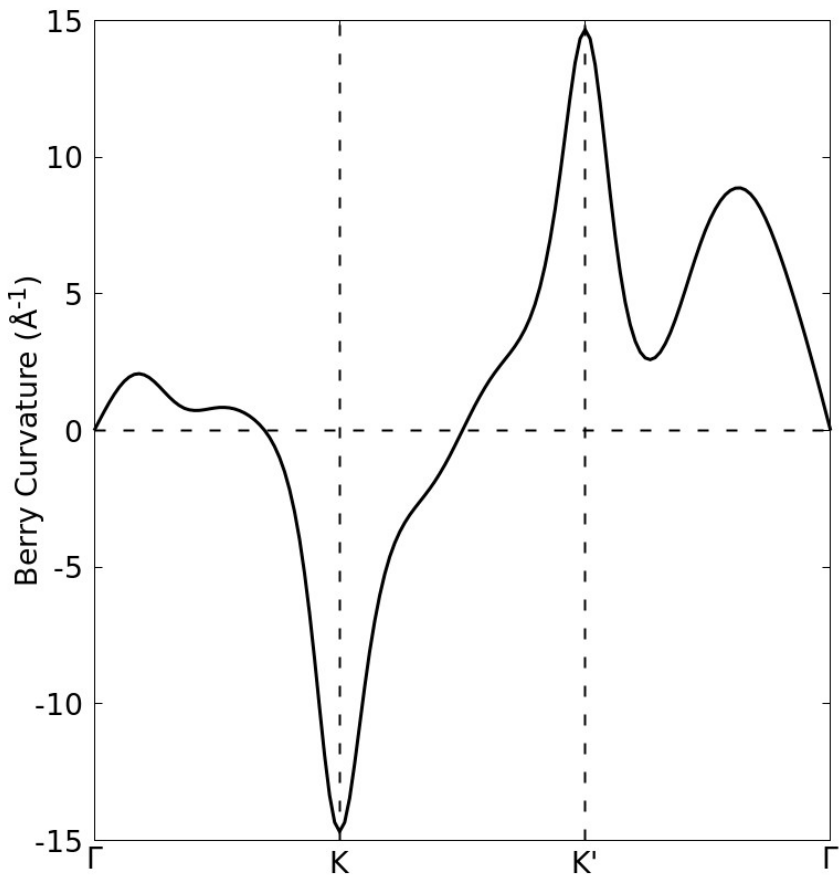
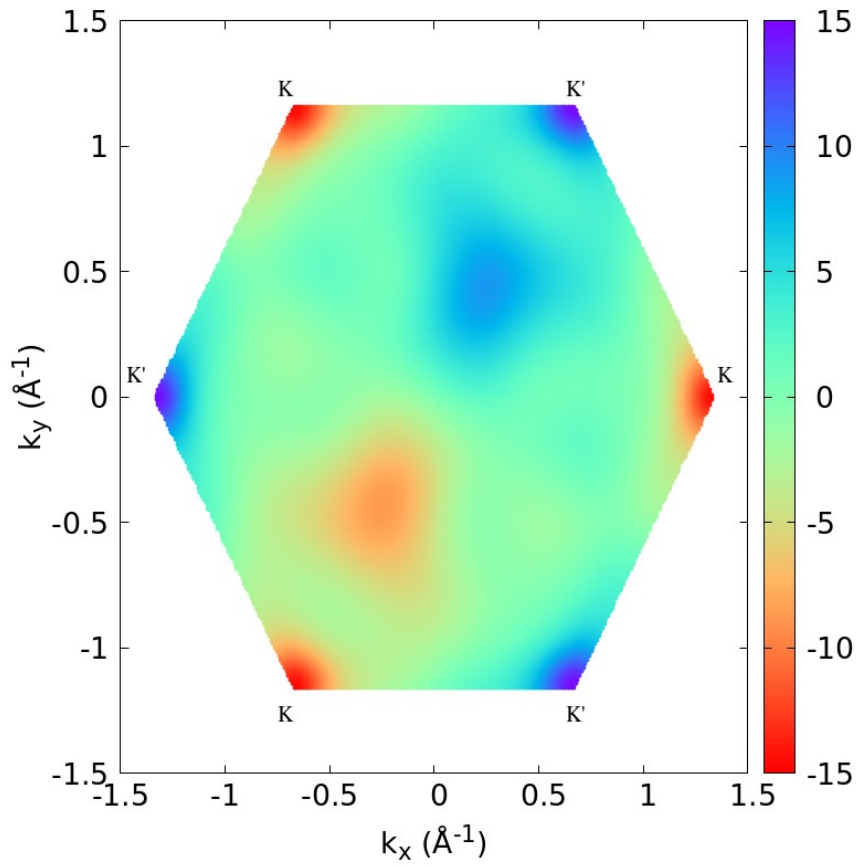
# Hands-On : Spin Texture



## Hands-On : Berry Curvature

```
1 NTHREADS= 8
2 SYSDIM= 2D
3 DFT= V
4
5 OUTPUT= './out/'
6 CALC_DATA= './out/'
7
8 PARAMS_FILE= 'tb_hr.dat'
9 KPATH_FILE= 'kpoints.dat'
10 KPATH_BSE= 'kpoints-bse.dat'
11
12
13 MESH_TYPE= "RK2D"
14 KMESH_GEN= "2DHEX"
15 RK= 400
16
17 BERRY_BZ= T
18 BERRY= T
19
```

## Hands-On : Berry Curvature



# Hands-On : Effective Mass Tensor

```
NTHREADS= 8
SYSDIM= "2D"
DFT= V

PARAMS_FILE= "tb_hr.dat"
KPATH_FILE= "kpoints.dat"
KPATH_BSE= "kpoints-bse.dat"
OUTPUT= "./out/"
CALC_DATA= "./out/"
EM_FILE= "cbm_vbm.dat"

EM_TENSOR= T
dK= 0.01400
```

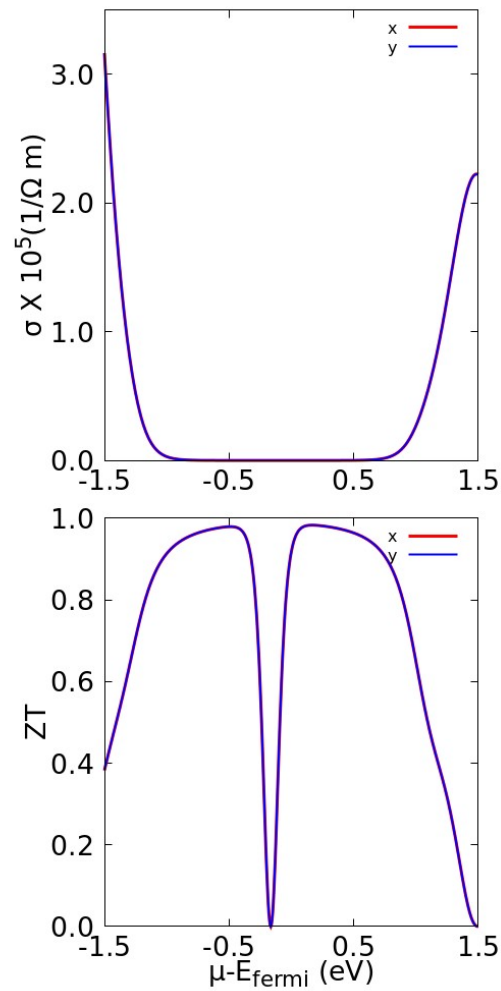
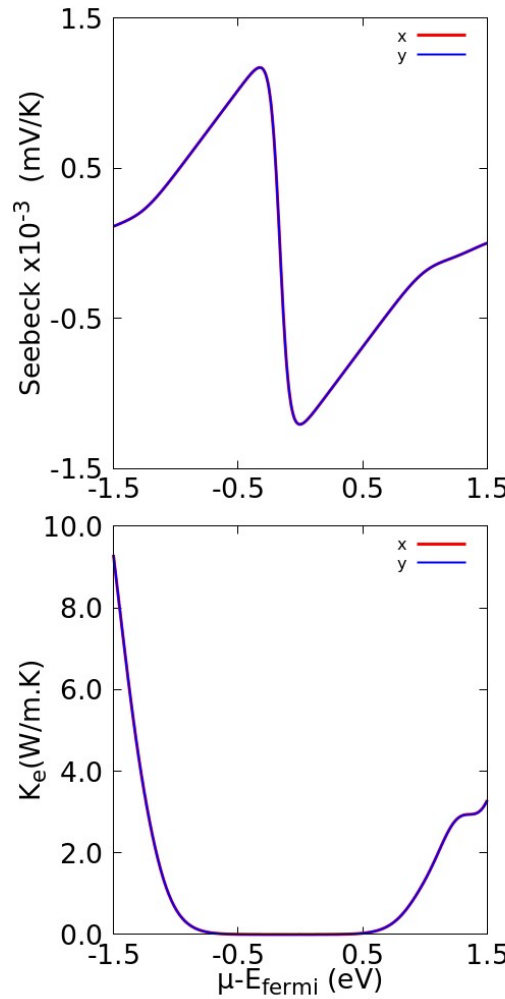
```
#####
# kx,ky,kz,band number,energy
1.3373 0.0000 0.000014 -1.2413
#####
Effective Mass Tensor
-0.4463 -159.2417
-159.2417 -0.4473
#####
# kx,ky,kz,band number,energy
1.3373 0.0000 0.000015 0.9523
#####
Effective Mass Tensor
0.3625 -62422.7578
-62422.7578 0.3623
#####
```

cbm\_vbm.dat

```
| 2
C
0.13373387E+01 0.59604645E-07 0.00000000E+00 14 -1.24131072
0.13373387E+01 0.59604645E-07 0.00000000E+00 15 0.95234990
```

# Hands-On : Thermoelectric Properties

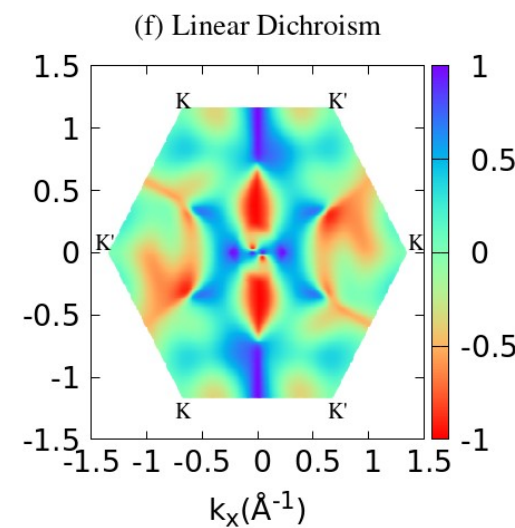
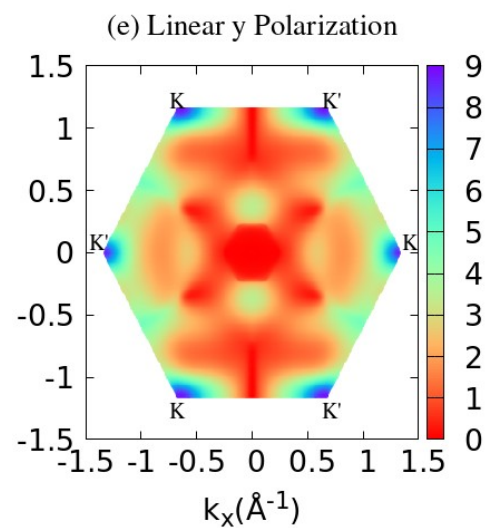
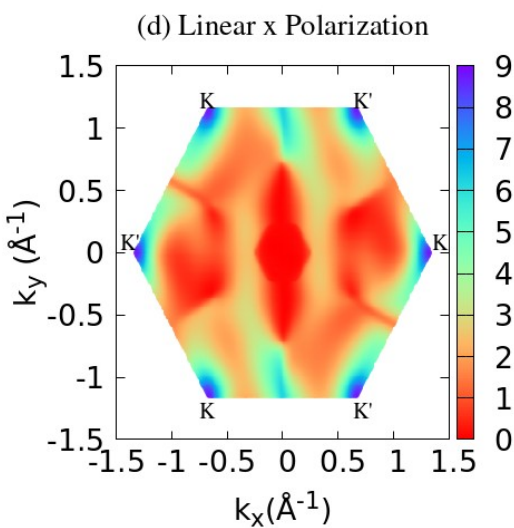
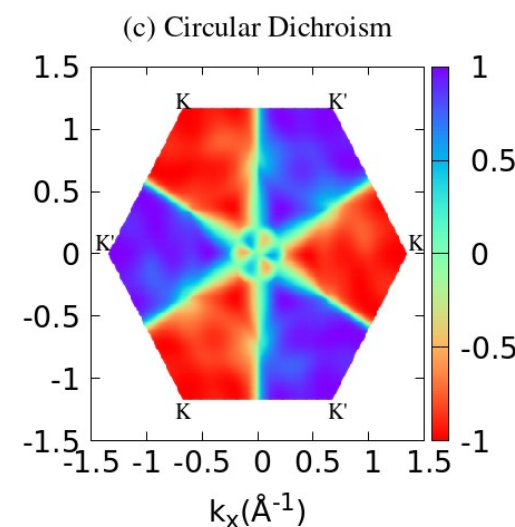
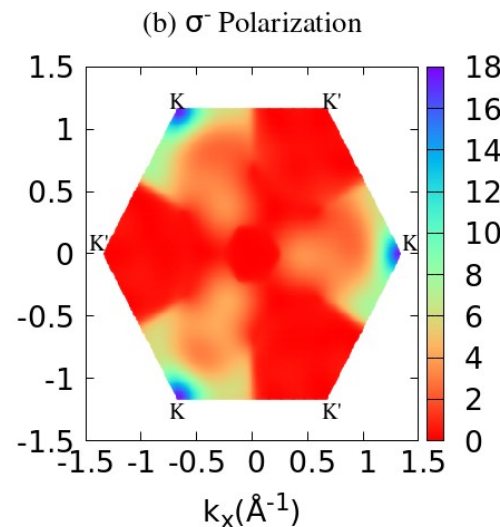
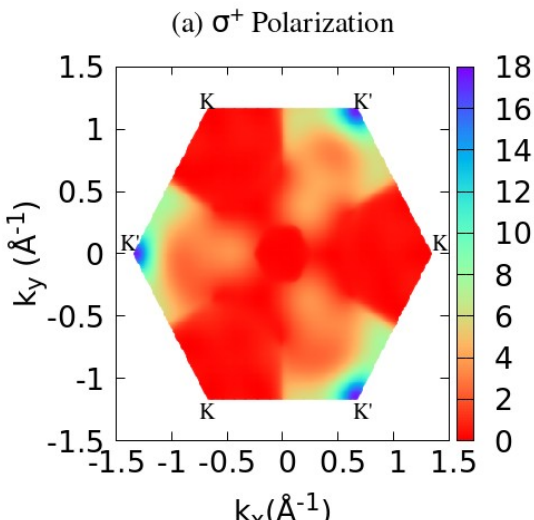
```
1 NTHREADS= 8
2 SYSDIM= "2D"
3 DFT= V
4
5 PARAMS_FILE= "tb_hr.dat"
6 KPATH_FILE= "kpoints.dat"
7 KPATH_BSE= "kpoints-bse.dat"
8 OUTPUT= "./out/"
9 CALC_DATA= "./out/"
10
11 BOLTZ= T
12
13 MESH_TYPE= "RK2D"
14 RK= 120
15
16 BTEMP= 900.0000
17 NEBOLTZ= 6001
18 NEMU= 601
19 MU_I= -1.50000
20 MU_F= 1.5000
21 KappaL= 0.00
22
23 ELFT_X= 2.48E-15
24 ELFT_Y= 2.48E-15
25 ELFT_Z= 2.48E-15
26 HLFT_X= 11.32E-15
27 HLFT_Y= 11.32E-15
28 HLFT_Z= 11.32E-15
```



## Hands-On : Optics in BZ (IPA)

```
1 NTHREADS= 8
2 SYSDIM= 2D
3 DFT= V
4
5
6 OUTPUT= './out/'
7 CALC_DATA= './out/'
8
9 PARAMS_FILE= 'tb_hr.dat'
10 KPATH_FILE= 'kpoints.dat'
11 KPATH_BSE= 'kpoints-bse.dat'
12
13
14 MESH_TYPE= "RK2D"
15 KMESH_GEN= "2DHEX"
16 RK= 400
17
18 OPT_BZ= T
19
20 NBANDSC= 2
21 NBANDSV= 2
```

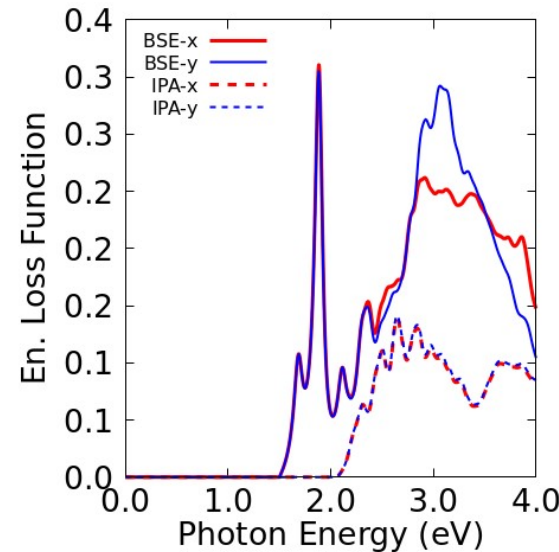
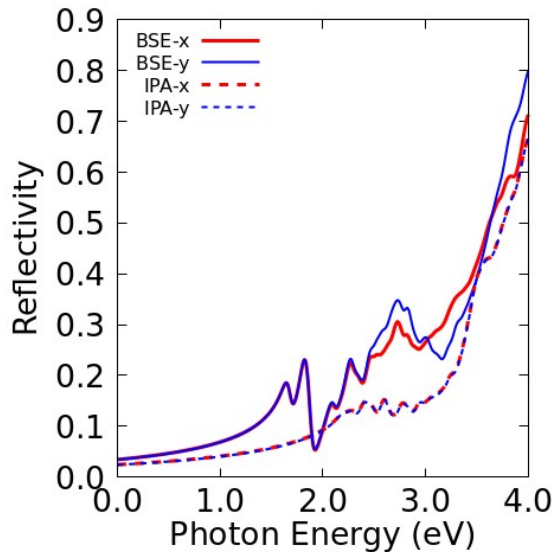
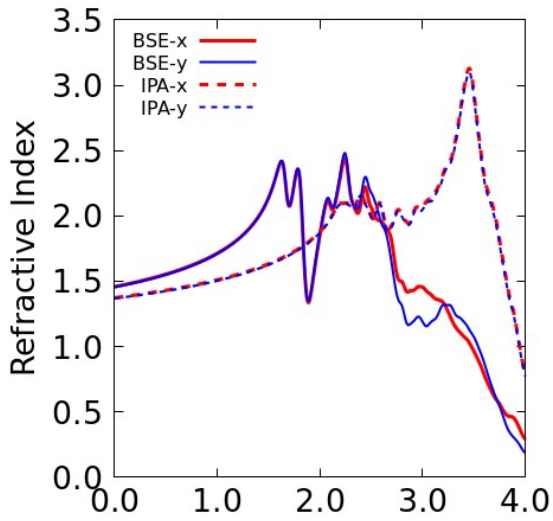
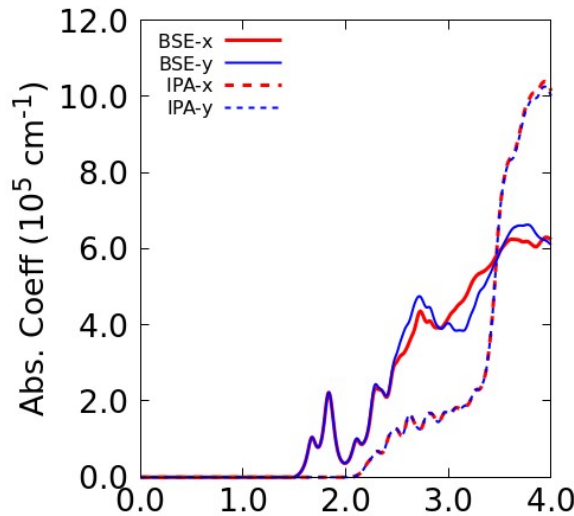
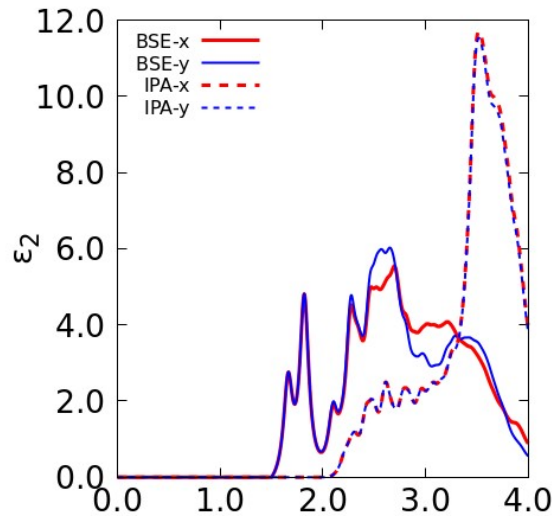
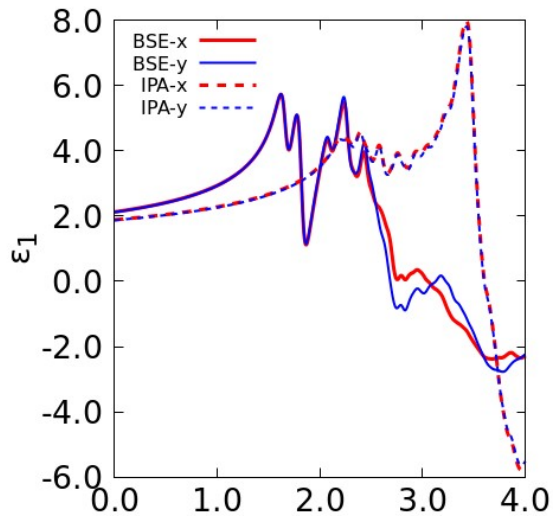
# Hands-On : Optics in BZ (IPA)



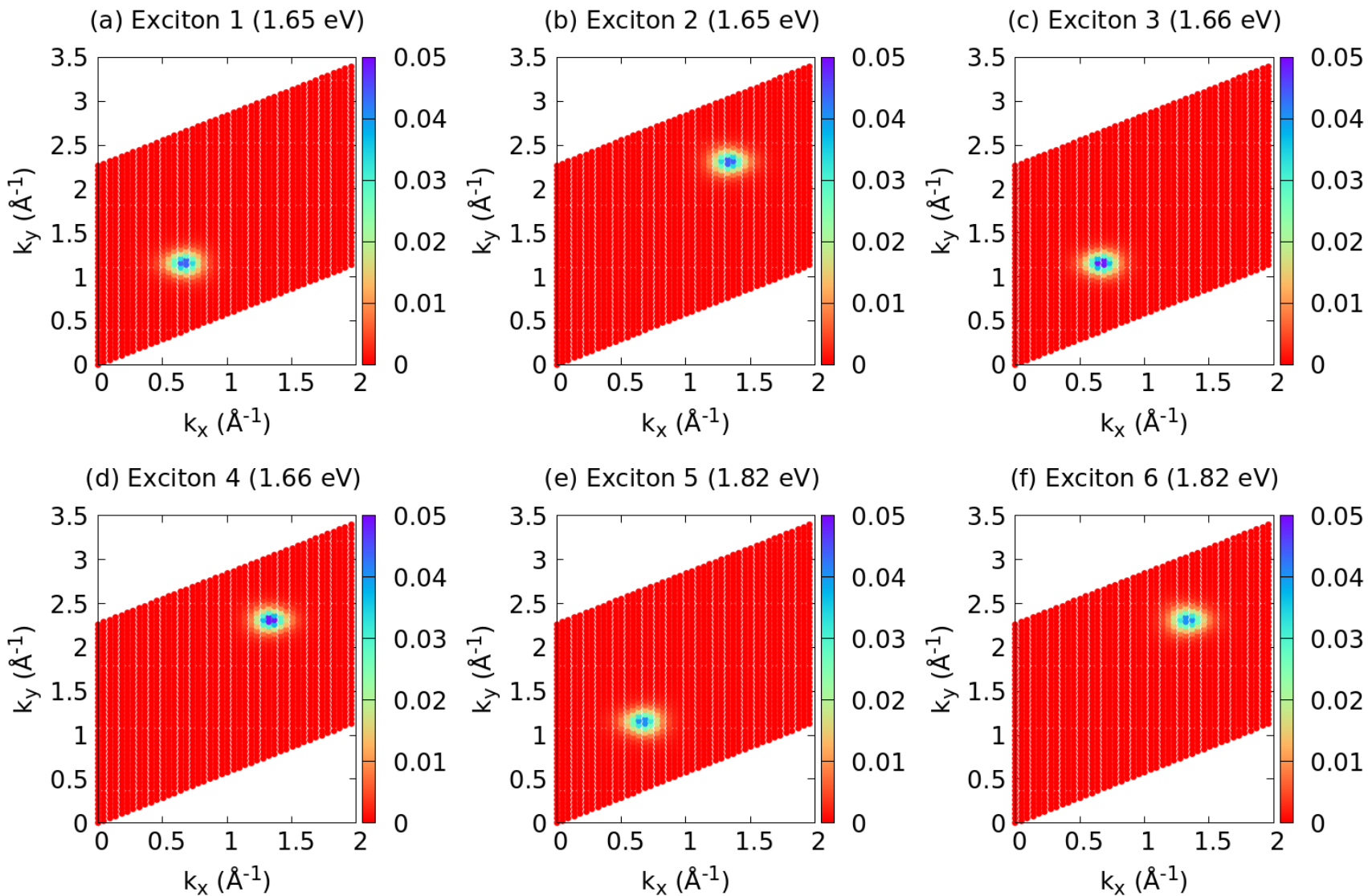
# Hands-On : Optical Properties

```
1 NTHREADS= 8
2 SYSDIM= '2D'
3 DFT= V
4
5
6 OUTPUT= './out/'
7 CALC_DATA= './out/'
8 PARAMS_FILE= 'tb_hr.dat'
9 KPATH_FILE= 'kpoints.dat'
10 KPATH_BSE= 'kpoints_bse.dat'
11
12 MESH_TYPE= RK2D
13 RK= 120
14
15 BSE_ALGO= cheevd
16
17 IPA= F
18 BSE= T
19 SPEC= T
20 TMCOEF= T
21 CPOL= T
22
23 PP_ONLY= F
24
25 BSE_WF= T
26 EXC_WF_I= 1
27 EXC_WF_F= 10
28
29
30
31 COULOMB_POT= V2DT
32 NBANDSC= 2
33 NBANDSV= 2
34
35 CSHIFT= 0.05
36 ENSPECI= 0.0
37 ENSPECF= 4.0
```

# Hands-On : Optical Properties



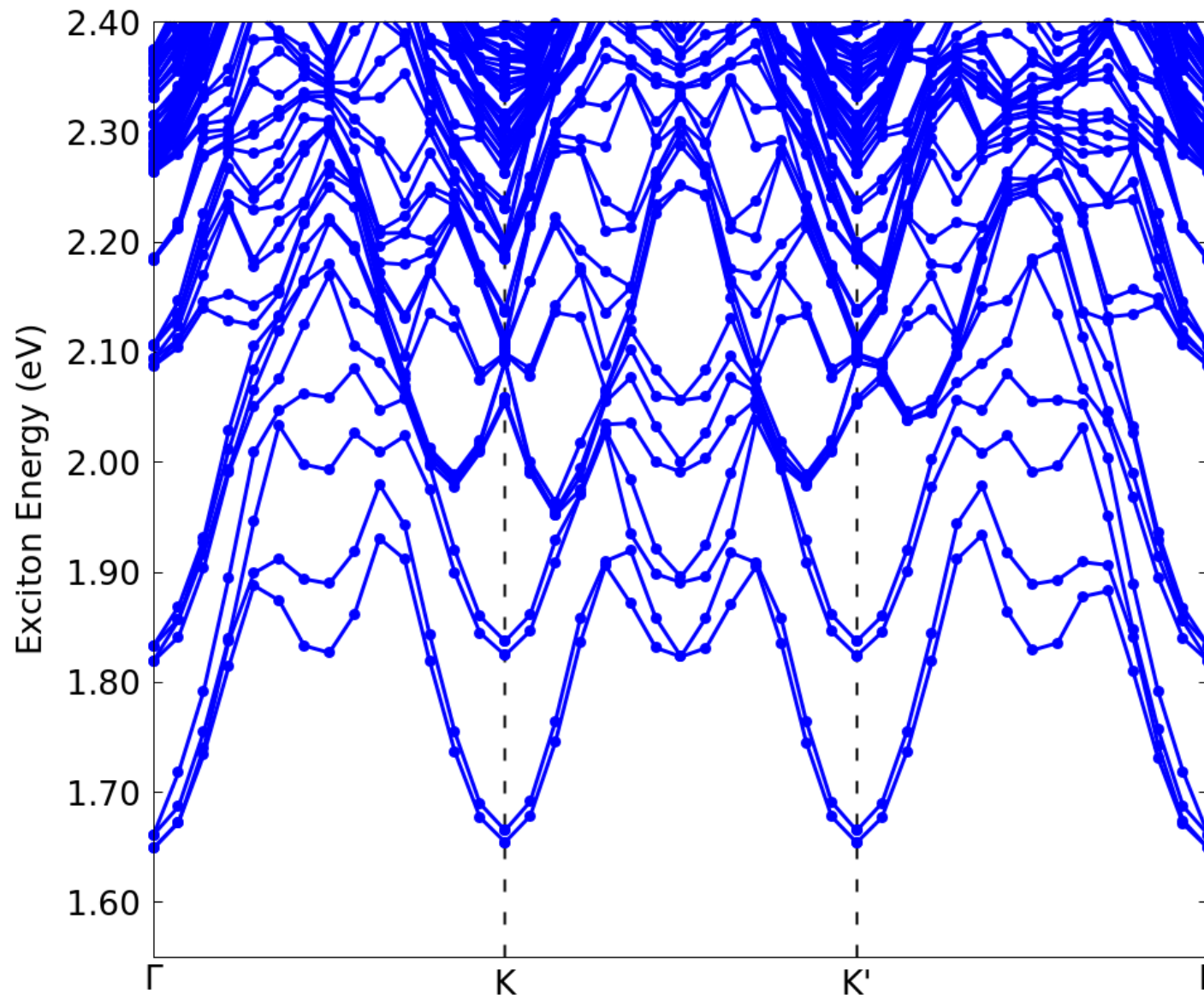
# Hands-On : Exciton Probability Density



## Hands-On : Exciton Band Structure

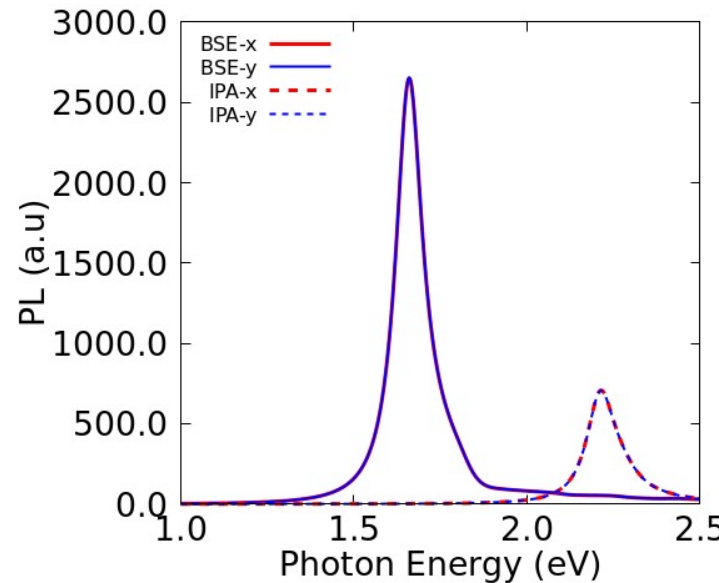
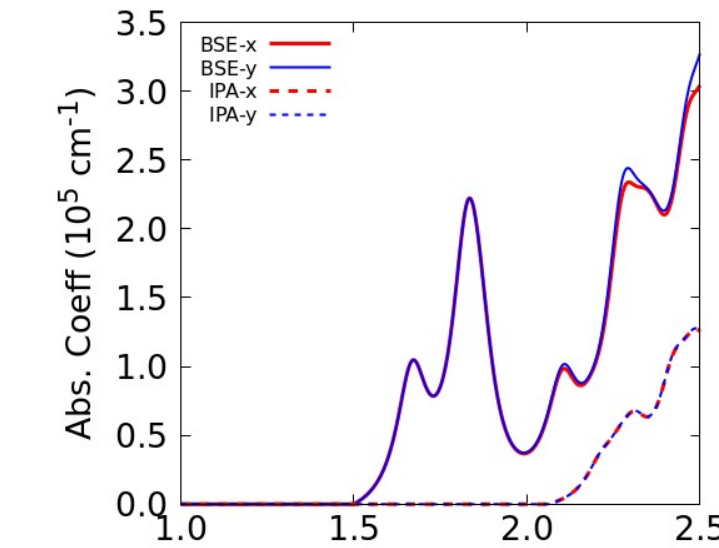
```
1 NTHREADS= 8
2 SYSDIM= '2D'
3 DFT= V
4
5
6 OUTPUT= './out/'
7 CALC_DATA= './out/'
8 PARAMS_FILE= 'tb_hr.dat'
9 KPATH_FILE= 'kpoints.dat'
10 KPATH_BSE= 'kpoints-bse.dat'
11
12 MESH_TYPE= RK2D
13 RK= 120
14
15 BSE_ALGO= cheevd
16
17 BSE_BND= T
18
19 COULOMB_POT= V2DT
20 NBANDSC= 2
21 NBANDSV= 2
22
```

## Hands-On : Exciton Band Structure



# Hands-On : Optical Properties (PL) + PCE

```
1 NTHREADS= 8
2 SYSDIM= '2D'
3 DFT= V
4
5 OUTPUT= './out/'
6 CALC_DATA= './out/'
7 PARAMS_FILE= 'tb_hr.dat'
8 KPATH_FILE= 'kpoints.dat'
9 KPATH_BSE= 'kpoints_bse.dat'
10
11 MESH_TYPE= RK2D
12 RK= 120
13
14 BSE_ALGO= cheev
15 BSE= T
16 SPEC= T
17 TMCOEF= T
18 CPOL= T
19
20 PP_ONLY= T
21
22 COULOMB_POT= V2DT
23 NBANDSC= 2
24 NBANDSV= 2
25
26 CSHIFT= 0.05
27 ENSPECI= 0.0
28 ENSPECF= 4.0
29
30 SES= AM15G
31 CTEMP= 300
32 THMAX= 6.4300E-10
33 EG= 2.193661
34 EGD= 2.193661
35 EGS= 1.649247
36 EBGS= 1.649247
37
```



# Hands-On : Optical Properties (PL)

## PCE-Limit-ipa.dat

```
| SQ-Limit
#Jsc: 107.108731258256 W/Vm^2
#Vmax: 1.74200439602137 V
#Voc: 1.85123253017664 V
#SQ-PCE 18.3792879300517 %
#FF 92.7236499288653 %

SLME-Limit
#Jsc: 107.108731258256 W/Vm^2
#Vmax: 1.74200439602137 V
#Voc: 1.85123253017664 V
#fr: 1.000000000000000
#SLME_max-PCE 18.3792879300517 %
#FF 92.7236499288653 %
```

## SLME-ipa.dat

```
#Jsc: 4.12154781458357 W/Vm^2
#Vmax: 1.77993488460779 V
#Voc: 1.88971176296473 V
#fr: 1.000000000000000
#SLME_max 0.722860324791301 %
#Thickness: 6.42999999999999E-004 micro m
#FF 92.8423585981839 %
```

## PCE-Limit-bse.dat

```
| SQ-Limit
#Jsc: 240.601504539016 W/Vm^2
#Vmax: 1.24105491787195 V
#Voc: 1.34166946560144 V
#SQ-PCE 29.2407139235346 %
#FF 90.6132656571181 %

SLME-Limit
#Jsc: 240.601504539016 W/Vm^2
#Vmax: 1.24105491787195 V
#Voc: 1.34166946560144 V
#fr: 1.000000000000000
#SLME_max-PCE 29.2407139235346 %
#FF 90.6132656571181 %
```

## SLME-bse.dat

```
#Jsc: 12.2950966694267 W/Vm^2
#Vmax: 1.26191692501307 V
#Voc: 1.36295356899500 V
#fr: 1.000000000000000
#SLME_max 1.51987484840185 %
#Thickness: 6.42999999999999E-004 micro m
#FF 90.7282438213983 %
```

## Features on Progress

- SIMSTACK interface
- FHI-aims interface
- DFTB interface
- G0W0 corrections
- Non-Linear Optics at IPA level
- Elastic Constants Post-Processing
- Electron-Hole Mobility Post-Processing
- Slack model for lattice thermal conductivity

# Publications using WanTiBEXOS

ACS APPLIED  
ENERGY MATERIALS

Open Access

This article is licensed under CC-BY 4.0

www.acsaem.org

Article

## Can 2D Carbon Allotropes Be Used as Photovoltaic Absorbers in Solar Harvesting Devices?

Alexandre Cavalheiro Dias,\* Carlos Derli Almeida Cornélio, Maurício Jeomar Piotrowski, Luiz Antônio Ribeiro Júnior, Carlos Maciel de Oliveira Bastos, Celso Ricardo Caldeira Rêgo, and Diego Guedes-Sobrinho\*



Cite This: ACS Appl. Energy Mater. 2024, 7, 8572–8582



Read Online

ACCESS |

Metrics & More

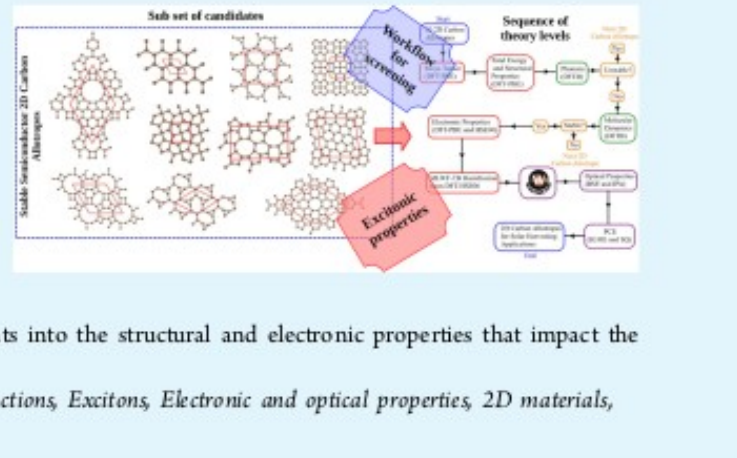
Article Recommendations

Supporting Information

andre Dias on October 14, 2024 at 14:16:42 (UTC).  
JELLINEs for options on how to legitimately share published articles.

**ABSTRACT:** Sustainable energy solutions have led to extensive research into materials for the conversion of solar energy. Two-dimensional carbon allotropes have garnered significant attention due to their unique structural and electronic properties, which can enhance the efficiency and sustainability of solar panels. This study used several computational methods, including density functional theory, density functional tight binding, and molecular dynamics simulations, to explore the solar energy conversion capabilities of 30 different 2D carbon-based allotropes. After a thorough analysis, we found that these materials exhibited a wide range of power conversion efficiency values, from 7% to 30%, assuming complete absorption of incident light. Our research provides valuable insights into the structural and electronic properties that impact the performance of these materials in solar cell applications.

**KEYWORDS:** Density functional theory, Tight-binding, Wannier functions, Excitons, Electronic and optical properties, 2D materials, Carbon allotropes



# Publications using WanTiBEXOS



Open Access

This article is licensed under CC-BY 4.0

Letter

pubs.acs.org/NanoLett

## Computational Characterization of the Recently Synthesized Pristine and Porous 12-Atom-Wide Armchair Graphene Nanoribbon

Djardiel S. Gomes, Isaac M. Felix, Willian F. Radel, Alexandre C. Dias, Luiz A. Ribeiro Junior, and Marcelo L. Pereira Junior\*



Cite This: *Nano Lett.* 2025, 25, 8596–8603



Read Online

ACCESS |

Metrics & More

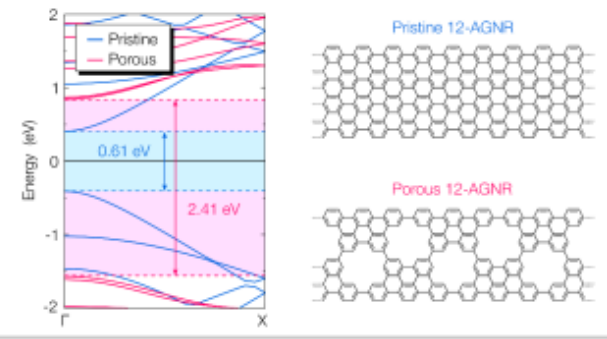
Article Recommendations

Supporting Information

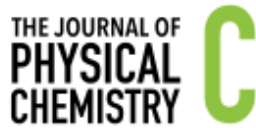
**ABSTRACT:** Recently synthesized porous 12-atom-wide armchair graphene nanoribbons (12-AGNRs) exhibit tunable properties through periodic porosity, enabling precise control over their electronic, optical, thermal, and mechanical behavior. This work presents a comprehensive theoretical characterization of pristine and porous 12-AGNRs based on density functional theory (DFT) and molecular dynamics simulations. DFT calculations reveal substantial electronic modifications, including band gap widening and the emergence of localized states. Analyzed within the Bethe-Salpeter equation framework, the optical properties highlight strong excitonic effects and significant absorption shifts. Thermal transport simulations indicate a pronounced reduction in conductivity due to enhanced phonon scattering at the nanopores.

At the same time, MD-based mechanical analysis shows decreased stiffness and strength while maintaining the structural integrity. Despite these modifications, porous 12-AGNRs remain mechanically and thermally stable. These findings establish porosity engineering as a powerful strategy for tailoring graphene nanoribbons' functional properties, reinforcing their potential for nanoelectronic, optoelectronic, and thermal management applications.

**KEYWORDS:** *graphene nanoribbons, porosity engineering, density functional theory, optical excitons, thermal transport, molecular dynamics*



# Publications using WanTiBEXOS



A JOURNAL OF THE AMERICAN CHEMICAL SOCIETY

pubs.acs.org/JPCC

Open Access

This article is licensed under CC-BY 4.0



Article

## Two-Dimensional Functionalized MM'CT<sub>2</sub> (M = Sc; M' = Y; T = Br, Cl, F, H, I, O, OH, S, Se, Te) MXene Monolayers for Photovoltaic Applications

Bill D. Aparicio-Huacarpuma,<sup>\*</sup> Enesio Marinho, Jr., José A. S. Laranjeira, William F. Giozza, Alysson M. A. Silva, Alexandre C. Dias, and Luiz A. Ribeiro, Jr.<sup>\*</sup>



Cite This: *J. Phys. Chem. C* 2025, 129, 13568–13580



Read Online

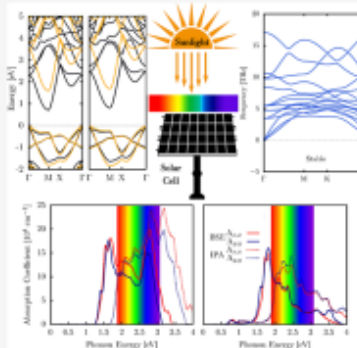
ACCESS |

Metrics & More

Article Recommendations

Supporting Information

**ABSTRACT:** We investigate the structural, optoelectronic, and excitonic properties of Janus bimetal MXene monolayers with the formula MM'CT<sub>2</sub> (M = Sc; M' = Y; T = Br, Cl, F, H, I, O, OH, S, Se, Te) using first-principles calculations combined with a semiempirical MLWF-TB+BSE approach. A developed workflow for a computational screening procedure was employed to assess their stability and optoelectronic performance. Excitonic and photovoltaic properties were computed using our group's WanTiBEXOS code, an open-source tool under active development and available under the GPL license. Among the 11 candidate monolayers, six were structurally stable semiconductors. Electronic band structure calculations indicate an indirect semiconducting nature for the majority of the compounds, with band gaps lying in the range of 0.96 eV to 1.90 eV. The linear optical response reveals a strong optical absorption in the infrared and visible regions, highlighting their potential for light-harvesting applications. Additionally, the calculated exciton binding energies range from 187 to 520 meV and are consistent with typical 2D materials, demonstrating significant excitonic effects for an accurate description of the optical band gap, a crucial property in the energy conversion process. The estimated power conversion efficiency, evaluated through the Shockley–Queisser limit, lies between 23.44% and 32.55%, at spectroscopy-limited maximum efficiency approach, it lies between 16.48% and 28.82%, when quasi-particle effects are considered, establishing these Janus MM'CT<sub>2</sub> MXenes as potential contenders for next-generation photovoltaic technologies.



# Publications using WanTiBEXOS

PHYSICAL REVIEW B 111, 235305 (2025)

## Optoelectronic properties of boron monochalcogenide monolayers: Quasiparticle and excitonic effects from first principles

Enesio Marinho, Jr.<sup>1,\*</sup> Alexandre C. Dias<sup>2</sup>, Lidia C. Gomes<sup>3</sup>, Antonio C. F. Seridonio<sup>1</sup>, Gabriel M. C. Meira<sup>1</sup>, Mariano de Souza<sup>4,5</sup>, Samuel M. Soares<sup>4</sup>, Lucas Squillante<sup>4</sup>, Pedro Venezuela<sup>6</sup>, Alexandre R. Rocha<sup>5</sup>, and Cesar E. P. Villegas<sup>7,†</sup>

<sup>1</sup>Departamento de Física e Química, Faculdade de Engenharia, Universidade Estadual Paulista (UNESP), Ilha Solteira-SP 15385-007, Brazil

<sup>2</sup>Instituto de Física e Centro Internacional de Física, Universidade de Brasília (UnB), Brasília-DF 70919-970, Brazil

<sup>3</sup>Departamento de Física, Universidade Federal de Pernambuco (UFPE), Recife-PE 50670-901, Brazil

<sup>4</sup>Departamento de Física, Instituto de Geociências e Ciências Exatas (IGCE), Universidade Estadual Paulista (UNESP), Rio Claro-SP 13506-970, Brazil

<sup>5</sup>Instituto de Física Teórica (IFT), Universidade Estadual Paulista (UNESP), São Paulo-SP 01140-070, Brazil

<sup>6</sup>Instituto de Física, Universidade Federal Fluminense (UFF), Av. Gal. Milton Tavares de Souza, s/n, 24210-346 Niterói, Rio de Janeiro, Brazil

<sup>7</sup>Departamento de Ciencias, Universidad Privada del Norte (UPN), Lima 15434, Peru



(Received 25 April 2025; revised 8 June 2025; accepted 11 June 2025; published 23 June 2025)

We investigate the linear optical response and excitonic landscape in boron monochalcogenide ( $BX$ ,  $X = S$ , Se, Te) single layers using *ab initio* many-body perturbation theory. These 2D monochalcogenides are wide band gap semiconductors, with the valence band exhibiting a quasiflat caldera-shaped dispersion in BS and BSe sheets, associated with strong van Hove singularities at the Fermi level in the density of states, an electronic feature that plays a crucial role in the emergence of strong excitonic effects. By solving the Bethe-Salpeter equation on top of  $G_0W_0$  quasiparticle energies, our results reveal that bound excitons arise from direct optical transitions between the highest occupied band and the lowest unoccupied band along the  $\Gamma - M$  and  $\Gamma - K$  paths. Additionally, in BS and BSe monolayers, we identify excitons that are bright for in-plane polarized incident light while becoming dark for out-of-plane polarization, and other excitons with the opposite behavior. The optical selection rules are described using group-theory analysis of wave-function symmetries, determining whether optical transitions are dipole allowed or forbidden. Furthermore, exciton radiative lifetimes are estimated to range from 0.2 ns to 1.6 ns at room temperature, while exciton binding energies are significantly high, ranging from 0.6 eV to 1.2 eV for both indirect ground-state excitons and zero-momentum direct excitons. Finally, the strong electron-hole interactions in these materials lead to the formation of tightly bound excitons with a small radius, paving the way for excitonic Bose-Einstein condensation in  $BX$  monolayers. Our study sheds light on the complex excitonic features of single-layer  $BX$ , emphasizing its potential for cutting-edge applications in exciton-driven optoelectronics and quantum technologies.

# Publications using WanTiBEXOS



pubs.acs.org/JPCC

Open Access

This article is licensed under CC-BY 4.0

Article

## Toward High-Efficiency Solar Cells: Insights into $\text{AsNCa}_3$ Antiperovskite as an Active Layer

Muhammad Irfan, Bill D. Aparicio-Huacarpuma, Carlos M. de Oliveira Bastos, Celso R. C. Rêgo, Diego Guedes-Sobrinho, Rafael Besse, Maurício J. Piotrowski, Alysson M. Almeida Silva, Alexandre C. Dias,\* and L. A. Ribeiro, Jr.



Cite This: <https://doi.org/10.1021/acs.jpcc.5c05620>



Read Online

ACCESS |

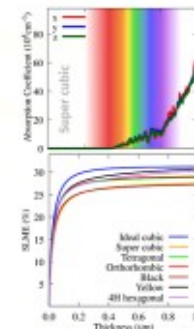
Metrics & More

Article Recommendations

Supporting Information

**ABSTRACT:** Advances in photovoltaic technology are a viable route for contributing to cleaner and more sustainable energy solutions, placing perovskite-based materials among the best candidates for solar energy conversion. However, some challenges must be addressed to enhance their performance and stability. Herein, we report an investigation of the  $\text{AsNCa}_3$  antiperovskite system for its potential in photovoltaic devices, using the density functional theory with semilocal and hybrid exchange–correlation functionals. We consider eight distinct crystalline phases, their structural parameters, dynamical stability, and electronic and optical properties. Furthermore, we consider each structural phase's contributions to solar harvesting efficiency by calculating the power conversion efficiency (PCE) using the spectroscopic

limited maximum efficiency formalism, which in this case reaches a maximum of 31.2%. All dynamically stable phases exhibit a band gap around ~1.3 eV, which lies within the optimal range for single-junction solar cells and yields PCE values comparable to the theoretical maximum PCE for silicon. These results place  $\text{AsNCa}_3$  antiperovskite as promising candidate for high-efficiency photovoltaic applications. Notably, the PCE is only slightly changed by structural phase modification, suggesting that phase transitions induced by environmental conditions during device operation might not compromise the device performance.



# Publications using WanTiBEXOS



Open Access

This article is licensed under CC-BY 4.0



<http://pubs.acs.org/journal/acsoff>

Article

## Exploring Novel 2D Analogues of Goldene: Electronic, Mechanical, and Optical Properties of Silverene and Copperene

Emanuel J. A. dos Santos, Rodrigo A. F. Alves, Alexandre C. Dias, Marcelo L. Pereira, Jr., Douglas S. Galvão, and Luiz A. Ribeiro, Jr.\*



Cite This: ACS Omega 2025, 10, 26892–26900



Read Online

ACCESS |

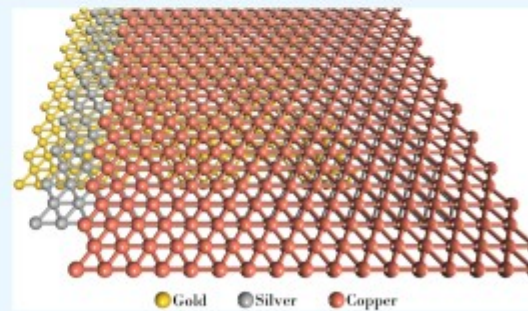
Metrics & More

Article Recommendations

Supporting Information

\*See options on how to legitimately share published articles.

**ABSTRACT:** Two-dimensional (2D) materials have garnered significant attention due to their unique properties and broad application potential. Building on the success of goldene, a monolayer lattice of gold atoms, we explore its proposed silver and copper analogues, silverene and copperene, using density functional theory calculations. Our findings reveal that silverene and copperene are energetically stable, with formation energies of  $-2.3$  and  $-3.1$  eV/atom, respectively, closely matching goldene's  $-2.9$  eV/atom. Phonon dispersion and ab initio molecular dynamics simulations confirm their structural and dynamical stability at room temperature, showing no bond breaking or structural reconfiguration. Mechanical analyses indicate isotropy, with Young's moduli of  $73$ ,  $44$ , and  $59$  N/m for goldene, silverene, and copperene, respectively, alongside Poisson's ratios of  $0.46$ ,  $0.42$ , and  $0.41$ . These results suggest comparable rigidity and deformation characteristics. Electronic band structure analysis highlights their metallic nature with variations in the band profiles at negative energy levels. Despite their metallic character, these materials exhibit optical properties akin to those of semiconductors, pointing to potential applications in optoelectronics.



# Publications using WanTiBEXOS

ACS APPLIED  
ENERGY MATERIALS

Open Access

This article is licensed under CC-BY 4.0

www.acsaem.org

Article

## Dispersive and Flat Electronic Bands in Two-Dimensional Triphosphides

Gabriel Elyas Gama Araújo, Lucca Moraes Gomes, Dominike Pacine de Andrade Deus,\* Alexandre Cavalheiro Dias,\* and Andréia Luisa da Rosa\*



Cite This: ACS Appl. Energy Mater. 2025, 8, 11548–11560



Read Online

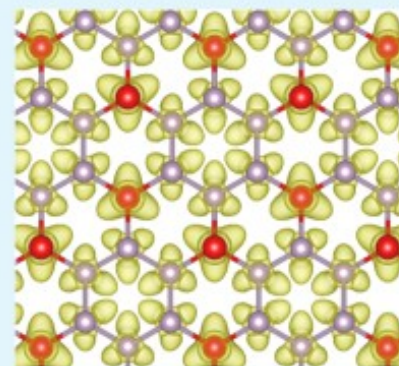
ACCESS |

Metrics & More

Article Recommendations

Supporting Information

**ABSTRACT:** In this work, first-principles density-functional theory and the Bethe-Salpeter equation (BSE) together with tight-binding-based maximally localized Wannier functions (MLWF-TB) have been used to investigate the structural, electronic, and optical properties of two-dimensional (2D) metal triphosphides ( $XP_3$ , X = Ga, Ge, As; In, Sn, Sb; Tl, Pb, and Bi). A noticeable feature is the appearance of flat and semiflat bands associated mainly with phosphorus atoms. Furthermore, molecular dynamics simulations show that these structures show a strong bond distortion at room temperatures, revealing the need for other stabilization mechanisms. Finally, we show that monolayered  $XP_3$  exhibits optical absorption with a strong excitonic effect, which makes these 2D materials promising candidates for future applications in electronic and photovoltaic devices.



**KEYWORDS:** 2D materials, phosphorus, excitons, flat bands, Bethe–Salpeter equation (BSE), molecular dynamics, density-functional theory

for options on how to legitimately share published articles.

# Publications using WanTiBEXOS



pubs.acs.org/JPCC

Article

## Theoretical Exploration of Structural and Excitonic Properties in Black Phosphorus: From First-Principles to a Semi-Empirical Approach

Diego Guedes-Sobrinho,\* Celso R. Caldeira Rêgo,\* Gabriel Reynald Da Silva, Henrique R. Da Silva, W. Wenzel, Maurício J. Piotrowski,\* and Alexandre Cavalheiro Dias\*



Cite This: <https://doi.org/10.1021/acs.jpcc.3c08414>



Read Online

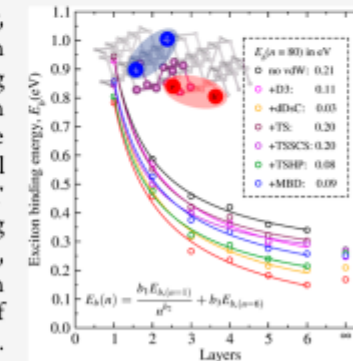
ACCESS |

Metrics & More

Article Recommendations

Supporting Information

**ABSTRACT:** Black phosphorus serves as an exemplary stacked bidimensional semiconductor, exhibiting anisotropic features in electronic and optical properties that demand special attention in theoretical investigations. Herein, we employed a series of computational protocols, starting with first-principles approaches (particularly density functional theory—DFT), combined with the solution of the Bethe–Salpeter equation within the tight-binding method to explore the structural stability and optoelectronic properties (bandgap, exciton binding energies, and optical absorption) of black phosphorus ( $P_n$ ) across layers ranging from  $n = 1$  to 6 and bulk. In our DFT investigations, we observed that empirical and semiempirical van der Waals models, contributing a dispersion energy component, revealed a myriad of differences and similarities in properties, such as interlayer nonbonded interactions. Notably, the many-body dispersion correction exhibited superior performance in connecting layered systems with the bulk. The magnitude of dispersion energies correlated with the stability during the aggregation process  $P_{(n-1)} + P_1 \rightarrow P_n$ . Additionally, the bandgap, properly corrected through relativistic quasi-particle calculations, narrowed due to enhanced interlayer wave function overlap, a result of the dispersion energies promoting the shortening of interlayer distances. Subsequently, we utilized the band structure relativistically corrected as a starting point to obtain the Hamiltonian, achieved through the generation of maximally localized Wannier functions. This facilitated a screening of the electron–hole (e–h) pairwise interaction Coulomb potential, specifically the exciton binding energy. We identified an indirect impact of the dispersion energies on excitonic properties, which were effectively described by the Rytova–Keldysh model for the e–h Coulomb potential, aligning well with photoluminescence experiments.



# Publications using WanTiBEXOS

Journal of Alloys and Compounds 1007 (2024) 176434



Contents lists available at ScienceDirect

## Journal of Alloys and Compounds

journal homepage: [www.elsevier.com/locate/jalcom](http://www.elsevier.com/locate/jalcom)



## Excitonic properties and solar harvesting performance of $\text{Cs}_2\text{ZnY}_2\text{X}_2$ as quasi-2D mixed-halide perovskites

Danilo Neves Silveira <sup>a,\*</sup>, Alexandre C. Dias <sup>b</sup>, Luis Octavio de Araujo <sup>a</sup>, Marco A.A. Queiroz <sup>a</sup>, Jônatas Favotto Dalmedico <sup>c</sup>, Carlos Maciel de Oliveira Bastos <sup>b</sup>, Celso R.C. Rêgo <sup>d</sup>, Maurício J. Piotrowski <sup>c</sup>, Diego Guedes-Sobrinho <sup>a,\*</sup>

<sup>a</sup> Department of Chemistry, Federal University of Paraná, Curitiba, PR 81531-980, Brazil

<sup>b</sup> Physical Institute and International Center for Physics, University of Brasília, Brasília, DF 70919-970, Brazil

<sup>c</sup> Department of Physics, Federal University of Pelotas, Pelotas, RS 96010-900, Brazil

<sup>d</sup> Institute of Nanotechnology Hermann-von-Helmholtz-Platz, Karlsruhe Institute of Technology, Karlsruhe 76021, Germany

---

### ARTICLE INFO

**Keywords:**

Metal halide perovskites (MHPs)

All-inorganic perovskite

Density functional theory

DFT-1/2

MLWF-TB

BSE

---

### ABSTRACT

Due to their low toxicity and high-temperature stability, lead-free quasi-2D metal halide perovskites (MHPs) are promising materials for optoelectronic applications. However, understanding their structural and optoelectronic properties, especially excitonic effects (electron-hole pair,  $e\text{-}h$ ), is challenging due to their quantum well topology. We propose an efficient protocol for band gap correction of  $\text{Cs}_2\text{ZnX}$  ( $X = \text{Cl}_4$ ,  $\text{Br}_2\text{Cl}_2$ , and  $\text{I}_2\text{Cl}_2$ ) and  $\text{Cs}_2\text{PbI}_2\text{Cl}_2$  (used as a benchmark) quasi-2D MHPs. This protocol is based on a relativistic quasiparticle approach (DFT-1/2) using density functional theory (DFT). We first examined the hybrid contributions of the halide alloys, leading to excitonic characterization using the Bethe–Salpeter equation within the maximally localized Wannier functions tight-binding method. This method provides a cost-effective approach for describing  $e\text{-}h$  quasiparticle effects. Additionally, we analyzed the crystal structure, thermodynamic stability, and optoelectronic properties of the newly synthesized Zn-based systems, focusing on their structural stability mechanisms. We found a correlation between the allocation of  $\text{Cs}^+$  cations in the crystal structure and the formation of two distinct stabilization patterns, influenced by the radii of the metal (Zn or Pb) and halide components. The relativistic correction of the band gap energies yielded results within 10 % of the experimental values. Furthermore, incorporating  $e\text{-}h$  quasiparticle effects for  $\text{Cs}_2\text{PbI}_2\text{Cl}_2$  resulted in an exciton binding energy of 0.160 eV, in excellent agreement with experimental data. This work represents a significant advance in the optoelectronic characterization of  $\text{Cs}_2\text{ZnX}$  systems, previously unexplored for their excitonic properties.

# Publications using WanTiBEXOS

Journal of Physics and Chemistry of Solids 182 (2023) 111573



Contents lists available at [ScienceDirect](#)

## Journal of Physics and Chemistry of Solids

journal homepage: [www.elsevier.com/locate/jpcs](http://www.elsevier.com/locate/jpcs)



## On the excitonic effects of the 1T and 1O<sub>T</sub> phases of PdS<sub>2</sub>, PdSe<sub>2</sub>, and PdSSe monolayers

Elie A. Moujaes <sup>a,\*</sup>, Alexandre C. Dias <sup>b</sup>

<sup>a</sup> Physics Department, Federal University of Rondônia, 76801-974, Porto Velho, Brazil

<sup>b</sup> University of Brasília, Institute of Physics, Brasília 70919-970, DF, Brazil

### ARTICLE INFO

**Keywords:**

2D materials  
Transition-metal dichalcogenides  
Excitons  
Density function theory

### ABSTRACT

We report the excitonic effects in the 1T and 1O<sub>T</sub> phases of PdS<sub>2</sub>, PdSe<sub>2</sub>, and PdSSe monolayers. Using fully relativistic norm-conserving non-local PBE pseudopotentials and including the spin-orbit (SOC) coupling, the 1T geometries are indirect band gap semiconductors; conversely, the 1O<sub>T</sub> structures are semimetallic. The band gaps were corrected using the HSE06 hybrid functional, making all structures semiconductors. Maximally localized Wannier functions were utilized to fit the bands of all six structures. The excitonic band structures were obtained using the Bethe-Salpeter equation (BSE), and the absorption coefficients were estimated at both the BSE and the independent particle approximation (IPA) levels. While the 1O<sub>T</sub> monolayers are more inclined to absorb light polarized in the y-direction, the 1T structures absorb light equally, independent of the polarization direction. We perceive that the 1T phase is the most promising candidate for photovoltaic devices; in particular, the 1T PdSSe system possesses a maximum power conversion efficiency (PCE) of 29.31 % if light trapping techniques are used to enhance absorbance. Amongst the 1O<sub>T</sub> materials, PdS<sub>2</sub> features the highest PCE of 8.38 %. Our results constitute the first step to encourage experimental studies towards the fabrication of Pd-based regular and Janus transition metal dichalcogenides photoabsorbers and give hints of how to increase the PCE of such materials.

# Signature of excitonic insulators in phosphorene nanoribbons

Andre Felipe Pereira de Oliveira<sup>1</sup>, Andréia Luisa da Rosa<sup>1,\*</sup> and Alexandre Cavalheiro Dias<sup>2</sup>

<sup>1</sup> Institute of Physics, Federal University of Goiás, Campus Samambaia, Goiânia, Goiás, 74690-900, Brazil

<sup>2</sup> Institute of Physics and International Center of Physics, University of Brasília, 70919-970 Brasília, Distrito Federal, Brazil

E-mail: [andreialuisa@ufg.br](mailto:andreialuisa@ufg.br)

Received 5 February 2024, revised 8 May 2024

Accepted for publication 14 May 2024

Published 28 May 2024



# Publications using WanTiBEXOS



Open Access

This article is licensed under [CC-BY 4.0](#)

<http://pubs.acs.org/journal/acsofd>

Article

## Raman Spectra and Excitonic Effects of the Novel $Ta_2Ni_3Te_5$ Monolayer

Alexandre C. Dias,\* Raphael M. Tromer, Humberto R. Gutiérrez, Douglas S. Galvão, and Elie A. Moujaes\*



Cite This: *ACS Omega* 2024, 9, 48835–48843



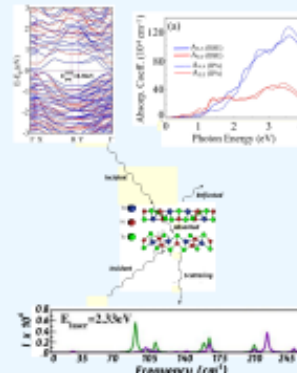
Read Online

ACCESS |

Metrics & More

Article Recommendations

**ABSTRACT:** We have investigated the Raman spectrum and excitonic effects of the novel 2D  $Ta_2Ni_3Te_5$  structure. The monolayer is an indirect band gap semiconductor with an electronic band gap value of 0.09 and 0.38 eV, determined using GGA-PBE and HSE06 exchange-correlation functionals, respectively. Since this structure is energetically, dynamically, and mechanically stable, it could be synthesized as a free-standing material. We identify 10 Raman- and 10 infrared-active modes for various laser energies, including those commonly used in Raman spectroscopy experiments. It was also observed that the contribution of Ni atoms is minimal in most Raman vibrational modes. In contrast, most infrared vibrational modes do not involve the vibration of the Ta atoms. As far as the optical properties are concerned, this monolayer shows a robust linear anisotropy, an exciton binding energy of 287 meV, and a high reflectivity in the ultraviolet region, which is more intense for linear light polarization along the  $x$  direction.



### PAPER



Cite this: *Dalton Trans.*, 2024, **53**,  
746

## Promising TMDC-like optical and excitonic properties of the TiBr<sub>2</sub> 2H monolayer†

André L. de O. Batista,<sup>a</sup> João Marcos T. Palheta, <sup>b</sup> Maurício J. Piotrowski, \*<sup>c</sup> Celso R. C. Rêgo, <sup>d</sup> Diego Guedes-Sobrinho<sup>e</sup> and Alexandre C. Dias \*<sup>f</sup>

The presented simulation protocol provides a solid foundation for exploring two-dimensional materials. Taking the TiBr<sub>2</sub> 2H monolayer as an example, this material displays promising TMDC-like optical and excitonic properties, making it an excellent candidate for optoelectronic and valleytronic applications. The direct band gap semiconductor (1.19 eV) is both structurally and thermodynamically stable, with spin-orbit coupling effects revealing a broken mirror symmetry in the K and K' valleys of the band structure, as confirmed by opposite values of the Berry curvature. A direct and bright exciton ground state was found, with an exciton binding energy of 0.56 eV. The study also revealed an optical helicity selection rule, suggesting selectivity in the valley excitation by specific circular light polarizations.

Received 23rd September 2023,  
Accepted 29th November 2023

DOI: 10.1039/d3dt03133k

rsc.li/dalton

# Publications using WanTiBEXOS

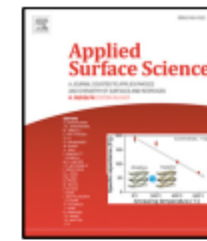
Applied Surface Science 696 (2025) 162831



Contents lists available at ScienceDirect

Applied Surface Science

journal homepage: [www.elsevier.com/locate/apsusc](http://www.elsevier.com/locate/apsusc)



Full length article

## Photocatalytic water splitting and excitonic effects of novel SiS<sub>2</sub>/SiSe<sub>2</sub> heterojunction

Shuai Lv <sup>a</sup>, Fujun Liu <sup>a</sup>,\*, Jinhua Li <sup>a</sup>, Vladimir V. Chaldyshev <sup>b</sup>, Alexandre C. Dias <sup>c,d</sup>,\*

<sup>a</sup> Nanophotonics and Biophotonics Key Laboratory of Jilin Province, School of Physics, Changchun University of Science and Technology, Changchun 130022, PR China

<sup>b</sup> Ioffe Institute, 26 Politekhnicheskaya str., St. Petersburg 194021, Russia

<sup>c</sup> Institute of Physics, University of Brasília, Brasília, 70910-900, Brazil

<sup>d</sup> International Center of Physics, University of Brasília, Brasília, 70910-900, Brazil

### ARTICLE INFO

#### Keywords:

First-principles calculations  
Van der Waals heterojunction  
Photocatalyst  
Excitons

### ABSTRACT

Energy crisis and environmental pollution require efficient photocatalysts for hydrogen production through hydrolysis and good photoabsorbers for solar energy conversion. Therefore, we designed a SiS<sub>2</sub>/SiSe<sub>2</sub> van der Waals heterojunction (vdWH) monolayer as a photocatalyst and photoabsorber. Based on first-principles calculations combined with semi-empirical maximally localized Wannier function tight-binding (MLWF-TB) method, it is revealed that SiS<sub>2</sub>/SiSe<sub>2</sub> vdWH is a semiconductor with an indirect band gap characterized by staggered band alignment, which facilitates the separation of electrons and holes, inhibiting electron-hole recombination. Additionally, the excitonic effects play a significant role in describing the linear optical response in these systems, resulting in an exciton binding energy closer to 300 meV and a small optical anisotropy surge. The solar harvesting analysis shows a solar harvesting efficiency closer to 20% in the vdWH, showcasing a performance enhancement when compared with the isolated monolayers. Our theoretical findings shed light on the design of novel nonmetal-based photocatalysts for water splitting and provide useful guidelines for future experiments.